Opto-Electronic Science

ISSN 2097-0382 CN 51-1800/O4

Optical trapping of optical nanoparticles: Fundamentals and applications

Fengchan Zhang, Pablo Camarero, Patricia Haro-González, Lucía Labrador-Páez and Daniel Jaque

Citation: Zhang FC, Camarero P, Haro-González P, Labrador-Páez L, Jaque D. Optical trapping of optical nanoparticles: Fundamentals and applications. *Opto-Electron Sci* **2**, 230019 (2023).

https://doi.org/10.29026/oes.2023.230019

Received: 3 July 2023; Accepted: 22 September 2023; Published online: 15 November 2023

Opto-Electronic Science

Review

September 2023, Vol. 2, No. 9

DOI: 10.29026/oes.2023.230019

Optical trapping of optical nanoparticles: Fundamentals and applications

Fengchan Zhang[1,2], Pablo Camarero[1,2], Patricia Haro-González[1,2,3], Lucía Labrador-Páez[4]* and Daniel Jaque[1,2,3]*

Optical nanoparticles are nowadays one of the key elements of photonics. They do not only allow optical imaging of a plethora of systems (from cells to microelectronics), but, in many cases, they also behave as highly sensitive remote sensors. In recent years, it has been demonstrated the success of optical tweezers in isolating and manipulating individual optical nanoparticles. This has opened the door to high resolution single particle scanning and sensing. In this quickly growing field, it is now necessary to sum up what has been achieved so far to identify the appropriate system and experimental set-up required for each application. In this review article we summarize the most relevant results in the field of optical trapping of individual optical nanoparticles. After systematic bibliographic research, we identify the main families of optical nanoparticles in which optical trapping has been demonstrated. For each case, the main advances and applications have been described. Finally, we also include our critical opinion about the future of the field, identifying the challenges that we are facing.

Keywords: optical trapping; optical nanoparticle; single particle spectroscopy; single particle sensor

Zhang FC, Camarero P, Haro-González P, Labrador-Páez L, Jaque D. Optical trapping of optical nanoparticles: Fundamentals and applications. *Opto-Electron Sci* **2**, 230019 (2023).

Introduction

In recent years, optical nanoparticles (ONPs) have become building blocks of modern photonics. An ONP can interact with light through processes of dispersion, absorption, and luminescence. These abilities have made them essential in numerous fields of application including solar energy[1–4], anti-counterfeiting[5–7], cosmetics[8], water treatment[9], biomedicine[10], etc. In most cases ONPs are sensitive to the conditions of the surrounding environment. This characteristic turns ONPs into remote sensors, as an appropriate analysis of their optical properties gives information about the physical-chemical properties of their environment without the need to establish physical contact between that environment and the measurement system. ONPs have been used as remote sensors for temperature[11–14], viscosity[15], chemistry[16–18], composition[19], and pressure[20]. Moreover, the lower limit of the spatial resolution that can be achieved when using an ONP as a sensor is the size of the ONP itself[21,22], i.e., below 100 nm. Reaching such nanometer resolution implies that the analyzed signal corresponds to an individual ONP. In most applications, however, the optical signal used for sensing is generated by multiple nanoparticles. In these cases, the spatial

[1]Nanomaterials for Bioimaging Group (nanoBIG), Departamento de Física de Materiales, Facultad de Ciencias, Universidad Autónoma de Madrid, 28049 Madrid, Spain; [2]Instituto de materiales Nicolás Cabrera, Universidad Autónoma de Madrid, 28049 Madrid, Spain; [3]Institute for Advanced Research in Chemical Sciences, Facultad de Ciencias, Universidad Autónoma de Madrid, 28049 Madrid, Spain; [4]Departamento de Química Física, Facultad de Ciencias Químicas, Universidad Complutense de Madrid, 28040 Madrid, Spain.

*Correspondence: L Labrador-Páez, E-mail: lulabrad@ucm.es; D Jaque, E-mail: daniel.jaque@uam.es

Received: 3 July 2023; Accepted: 22 September 2023; Published online: 15 November 2023

resolution of the measurement is determined by that of the optical system used for detection. For example, when ONPs are used as sensors in cells, the resolution of the measurement is limited by the resolution of the optical microscopes, typically in the order of the micrometer. Therefore, achieving nanometer resolutions when using ONPs as sensors requires single particle spectroscopy (SPE) techniques. SPE studies on ONPs allow to achieve not only nanometric spatial resolutions, but also reliable calibrations of ONPs as sensors. When the analyzed optical signal comes from many ONPs, any variation in the detected optical signal may be caused not only by changes in their environment but also by the interaction between ONPs[23,24]. In other words, when the optical signal generated by many ONPs is analyzed, bias mechanisms may interfere to the extent of reducing the reliability of the sensor. Therefore, to achieve reliable and high-resolution measurements based on ONPs, it is necessary to assess the luminescence of individual ONPs through SPE techniques.

SPE is relatively easy when ONPs are immobilized on a substrate. In these cases, it is "just" necessary to localize the ONPs by additional techniques (such as scanning tunneling microscopy[25,26] or atomic force microscopy[27–29]) to subsequently analyze their optical properties using conventional optical systems. If the separation between ONPs is greater than the resolution of the optical system, it is possible to access to the optical response of a single ONP. The situation, however, becomes more complicated when it is intended to make SPE of a colloidal single ONP. In this case the Brownian motion of the ONPs makes it impossible to immobilize them, to assess their optical signal. SPE of colloidal ONP requires a technology capable of immobilizing a single ONP in aqueous solutions while its optical properties are analyzed. In this sense, Optical Tweezers (OTs) seem to be the ideal solution. In its basic configuration, OTs consist of a focused laser beam. Due to the optical forces that appear in the surrounding of the beam focus, colloidal particles in its surroundings are attracted towards it. Once within the laser focus, they remain immobilized provided the optical potential created by the focused laser beam is larger than the thermal energy ($k_B T$) of the colloidal particle[30]. Since it is a pure optical technique, it opens the possibility of analyzing the optical signal (transmission, scattering, or luminescence) of the trapped ONP by coupling the system to a spectrometer. Although optical trapping of microparticles is relatively easy, indeed optical trapping was firstly discovered in microparticles by A. Ashkin in 1970[31], trapping of ONPs becomes challenging. When the size of the trapped particle is much larger than the wavelength of trapping radiation, optical forces that appear due to transfer of momentum can be as large as nanonewtons. However, when dealing with nanoparticles, the particle size is much smaller than the wavelength of trapping radiation. The optical force arises from the interaction of the polarized particle and the field gradient. In these conditions the optical force, $F_{\rm opt}$ can be written as[32]:

$$F_{\rm opt} = \frac{1}{4}\varepsilon_0 \alpha \nabla E^2 \ , \tag{1}$$

where ε_0 is the dielectric constant of vacuum, α is the real part of ONP electronic polarizability, and $E^2 = EE^*$ being E the electric field of trapping radiation.

Due to the reduced electronic polarizability of nanosized particles, optical forces acting on nanoparticles are in the order of piconewtons, which can be considered as weak. Furthermore, the stability of the optically trapped nanoparticles is generally compromised by the thermal energy of nanoparticles (Brownian motion could make the nanoparticles to escape from the trap). To date, various methods have been developed to improve the optical forces and thus the stability of optically trapped nanoparticles. These methods can be classified as based on increasing either the electronic polarizability (α) of the nanoparticle or the magnitude of the electric field (E) of trapping radiation. The electric polarizability of nanoparticles can be increased by enhancing their zeta potential via adequate surface modification[33,34]. The enhancement of E term in expression (1) requires the improvement to the optical trapping setup, for instance, plasmonic nanostructures[35–37], photonic resonators[38,39] or microlenses[40,41]. Additionally, single particle trapping requires the use of very diluted colloids so the probability of multiparticle events is minimized. The drawback of working with such diluted suspensions is that the frequency of trapping events is very low. Therefore, it can take several minutes to incorporate a single nanoparticle into the trap. Despite optical trapping of a single nanoparticle is challenging, numerous works have demonstrated that optical trapping of individual nanoparticles is possible[42]. Furthermore, it has been demonstrated how it is feasible to assess the optical properties of ONPs while being isolated by an OT[23]. This makes remote sensing at the nanoscale possible.

Despite the promising results reported by pioneering

works, the use of OTs for SPE of ONPs is still in its infancy. Bibliographic research reveals the limited number of reports on optical trapping of individual ONPs belonging to different families (ranging from plasmonic nanoparticles to nanodiamonds), in diverse experimental configurations, and for a great variety of applications (from thermal sensing to single particle dynamics). The next steps towards improving the results obtained so far require a critical analysis of the state of the art, discussion about the solutions to challenges proposed by different authors, the advances in the design of the experimental set-up, and the adequate selection of the nanoparticle depending on the intended application.

In this review article we aim to summarize the main results published so far in the optical trapping of single ONPs so that novel researchers get a general view of the state of the art while experienced researchers can get in a shot all the information to design their future experiments. The review is structured in two sections in addition to this introduction. In Section *Optical trapping of single ONPs*, according to different materials and their optical properties, the ONPs are classified into five families: plasmonic nanoparticles, lanthanide-doped nanoparticles, polymeric nanoparticles, semiconductor nanoparticles, and nanodiamonds. For each case we have described the experimental set-ups used, the applications developed, and the challenges faced. In Section *Conclusions and perspectives* we include a critical analysis of the state of the art based on the results highlighted in Section *Optical trapping of single ONPs* and we include our personal view of the future of the field.

Optical trapping of single ONPs

As mentioned in the introduction, optical trapping and manipulation at the single particle level has been demonstrated in a great variety of systems, under different experimental approaches, and for diverse applications. To give a general idea of the state of the art and the challenges the field is finding, we have grouped the results obtained so far according to the material constituting the ONPs optically trapped and employed as sensor. According to this criterium, we have classified the results obtained so far into 5 different groups: plasmonic nanoparticles, lanthanide-doped nanoparticles, semiconductor nanoparticles, polymeric nanoparticles, and nanodiamonds.

Plasmonic nanoparticles

The optical trapping forces experienced by plasmonic nanoparticles (PNPs) are usually larger than for dielectric nanoparticles of the same size due to their larger polarizability (7.33×10^{-17} cm^3 for 36 nm diameter gold nanosphere)[43]. Such superior polarizability obeys to the coupling of the electric field of light and the surface plasmons, i.e. the collective resonant oscillations of the electrons of the conduction band of the metal[44]. Indeed, when the wavelength of incident light matches the plasmon resonance of the PNP, it may lead to enhanced light absorption, Rayleigh light scattering, and intense local field enhancement near the surface[44]. PNPs' large polarizability is not only wavelength-dependent, but it also varies with the particle shape, volume, frequency-dependent dielectric response of the metal, and refractive index of the environment. The optical gradient force results large and attractive when the metallic particle is trapped by light with a lower frequency than the plasmon resonance and repulsive if it has a larger frequency. Therefore, the selection of the optical trapping laser wavelength is critical for this type of nanomaterials. Another crucial point for this type of ONP is their inherent high light-to-heat conversion efficiency. When the collective motion of electrons is excited, the subsequent electron relaxation via Joule effect leads to heat generation. This may lead to deleterious Brownian thermal motion and reduce the stability in the optical trap. An increase in the local temperature may reduce the viscosity of the medium surrounding the PNP. This in turn reduces the hydrodynamic resistance acting on the PNP, allowing it to escape from the OT. Thus, local heating may interfere with the ongoing research or application[44,45].

Despite the difficulties listed above, OT of PNPs has been achieved by different groups in a great variety of configurations. Typical applications of optically trapped metallic nanoparticles are based on: spinners[46], single-molecule surface-enhanced Raman spectroscopy (SERS)[47], particle-particle interaction (dimers)[48], and temperature sensing[49]. In this section we limit the scope to overview the main results obtained in the last two of those applications, as they are the only ones based on the optical properties of the trapped PNPs. For that purpose, usually darkfield spectroscopy or imaging devices are coupled to the optical tweezer setup. That can be easily achieved by adding illumination with a cone of light and then spectrally analyzing the light scattered by the PNP or by performing hyperspectral imaging of the optical trap, respectively[50,51]. In that way, single PNP scattering spectra can be recorded[52,53].

Temperature sensing with optically trapped plasmonic nanoparticles

Some nanoparticles, including plasmonic nanoparticles, behave as optical nanothermometers. An optical nanothermometer is a nanoparticle whose optical properties are strongly temperature dependent so the analysis of the radiation absorbed, scattered, or emitted by the nanoparticle can be used to obtain a remote thermal readout. As we will describe in Section *Thermal sensing with an optically trapped lanthanide-doped nanoparticle* and Section *Fluorescent nanodiamonds*, lanthanide-doped nanoparticles and nanodiamonds can also behave as thermal sensors when being optically trapped. The comparison of the different nanothermometers can be found in previous reviews[54–56].

As it was mentioned previously, the plasmon resonance wavelength of a PNP depends on the refractive index of surrounding medium, which in turn depends on temperature. Thus, measuring the variation of the plasmon resonance wavelength of a single PNP provides information about the medium temperature so that the PNP becomes a remote thermal sensor. Usually, an increment in the medium temperature is detected by a blueshift of the plasmon resonance. The easiest way to determine the plasmon resonance wavelength of an individual PNP is to immobilize it on a substrate. However, the temperature of a PNP deposited over a substrate may be different depending on the material of the substrate, which may act as a heat dissipator and have a variation of refractive index with temperature different from that of the medium[57]. For that reason, if a PNP is to be used as a thermal sensor, it should be kept away from the substrate, i.e. the PNP has to be isolated and analyzed while being suspended in the medium by an OT. Optical manipulation of individual PNPs opens the possibility of an alternative way for remote thermal sensing through the scattering spectra of the trapped PNP, which can be monitored by darkfield spectroscopy. However, in these cases there is a risk that their large light-to-heat conversion efficiency may alter the temperature reading by artifactually increasing the temperature of the sensor itself[50].

Alternatively, temperature can be estimated by the rotation of the PNP within the optical trap, as the spinning velocity is determined by the temperature-dependent medium viscosity. Spinning originates because light can exert torque on an object through absorption and scattering. In the case of the spinning of PNPs, the angular momentum is in general maximized for trapping wavelengths close to the plasmon resonance[46]. However, the self-heating of PNPs due to their absorption of the trapping laser may alter the viscosity of the fluid around it, and therefore its rotation speeds may experience artefacts in temperature estimation[49,58].

The most representative example of the potential of optically trapped PNP for thermal sensing is the work published by D. Andrén et al.[49] They employed gold nanorods as optically trapped nanothermometers. They monitored both the longitudinal plasmon wavelength by darkfield spectroscopy and the spinning velocity to determine the temperature of an individual gold nanorod within an optical trap. Both methods rendered similar results for the estimated temperature (Fig. 1(a, b)). Through this process they observed a slight deviation in the tendency of the plasmon wavelength with temperature. They observed that the gold nanorod was producing so much heating over certain threshold of trapping laser

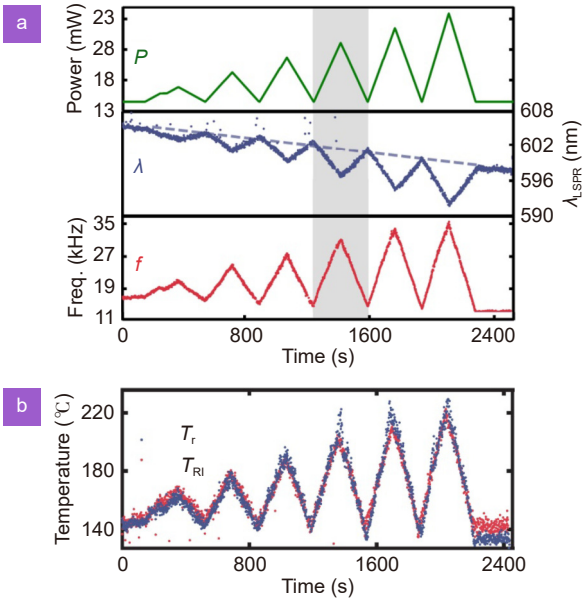

Fig. 1 | (**a**) Time evolutions of the longitudinal surface plasmon resonance (LSPR) peak position (blue points) and the rotation frequency (red) as the laser power (green) is swept in sawtooth ramps with linearly increasing maxima. The dashed blue line is fit to the low laser power spectral peak positions, illustrating the continuous reshaping behavior. The grey area indicates a change in the slope of the linear relation between the laser power and λ_{LSPR}, where nucleation of vapor is suggested to occur. (**b**) Temperature determination based on LSPR spectroscopy (red data points, based on water's refractive index (RI) temperature variation and subsequent λ_{LSPR} variation) and rotational Brownian dynamics (blue data points, based on water's viscosity temperature variation and subsequent rotation frequency change) obtained from the data in (a). Figure reproduced with permission from ref.[49], Copyright 2017 American Chemical Society.

power, that it experienced a progressive reshaping, leading to rods of a lower aspect ratio.

Nanoparticle-nanoparticle interaction

When two PNPs approach each other forming a dimer, their coupling leads to a shift of the resulting surface plasmon resonance towards lower energy (Fig. 2(a–f)) and to a significant increment of the intensity of the scattered light. This phenomenon also creates a hot spot, i.e., a region of intense electric field in between the interacting PNPs. Such a hot spot can be used to enhance the Raman signal or the fluorescence of a fluorophore, making plasmonic dimers useful for applications in single-molecule spectroscopy and sensing[47,59]. Next we highlight the most relevant works dealing with the use of optical traps for the study of the formation, dynamics, and applications of plasmonic dimers.

Optical traps are an ideal tool to study the formation of plasmonic dimers, as they allow the controlled approaching of the interacting PNPs and their simultaneous characterization by darkfield spectroscopy. A. Ohlinger et al.[48] observed the sequential incorporation of silver nanospheres to an optical trap (Fig. 2(a)) and recorded a spectral shift of over 100 nm (Fig. 2(b)), supported by the simulated spectra in (Fig. 2(c)), due to the formation of a dimer of PNPs within the optical trap. Such a large variation of the plasmon resonance wavelength can be detected even by simply observing the color of the light scattered by the PNPs in the optical trap by means of a CCD camera coupled to the set-up (Fig. 2(d–f)). However, the formation of dimers also implies an enhancement of the heating produced by the trapped particles, which destabilizes them in the optical trap. Later, H. Kermani et al.[60] demonstrated that a dimer of

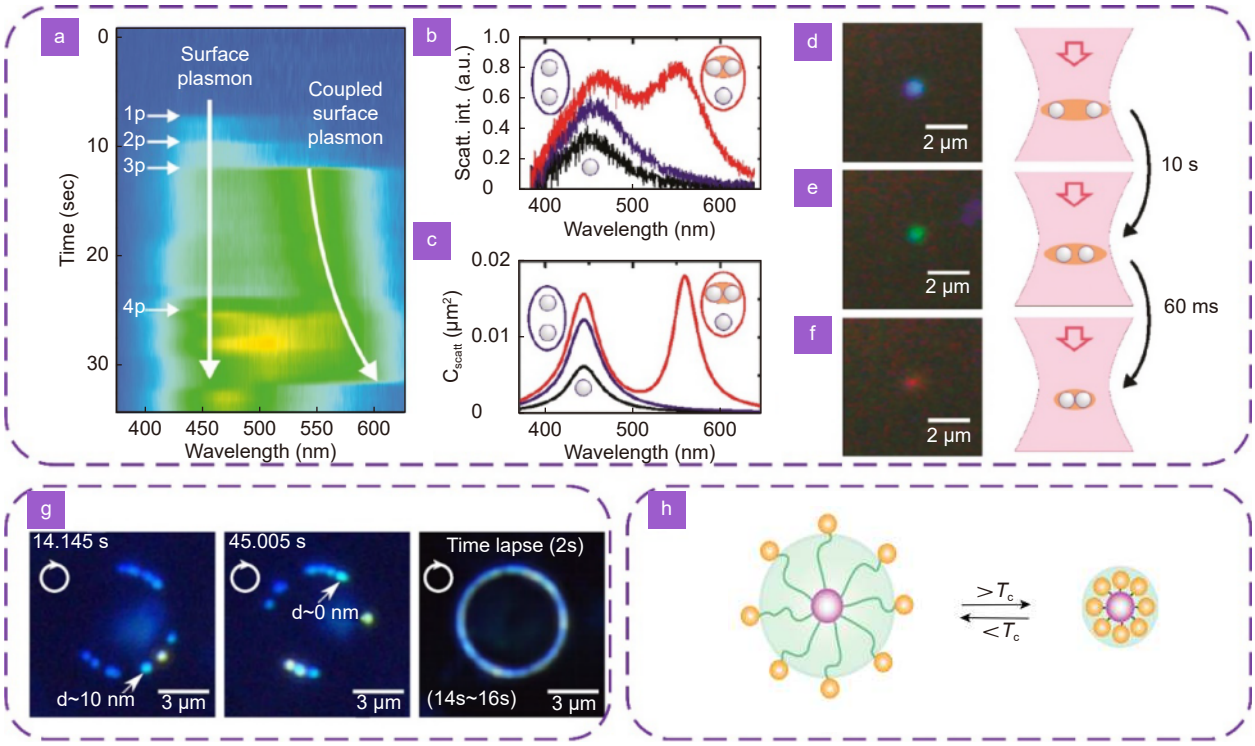

Fig. 2 | Plasmonic nanoparticles for investigation of nanoparticle-nanoparticle interaction. (**a**) Time evolution of the darkfield spectrum of optically trapped silver nanoparticles. Observing intensity steps at the silver plasmon resonance (~450 nm) allowed to count the number of nanoparticles entering inside the trap. (**b**) Experimental darkfield spectra of one (black), two noncoupled (blue), and three (two of them coupled) (red) trapped silver nanoparticles. (**c**) Theoretical plane wave scattering cross section spectra of one (black), two noncoupled (blue), and two coupled (distance = 2 nm) plus one noncoupled (red) silver nanoparticles, assuming randomly changing orientation of nanoparticles in space. Evolution of scattering color at the optical trap (true color images) with time when two silver nanoparticles are simultaneously trapped: (**d**) initially, (**e**) 10 s after (d), (**f**) 60 ms after (e). No other particles were observed entering the trap during the color evolution process. (**g**) Darkfield images at different times (left and center) and time-lapse image (right) illustrating the optical transport of several 60 nm diameter silver nanospheres around a 3 μm radius ring-shaped optical trap. Darker blue for monomers, lighter blue for close-standing nanospheres, light green for dimers. (**h**) Illustration of the thermo-responsive behavior of the core (purple)-satellite (orange) plasmonic nano-assemblies incorporating thermo-responsive polymers. Figure reproduced with permission from: (a–f) ref.[48], Copyright 2011 American Chemical Society; (g) ref.[62], Copyright 2021, Chinese Laser Press.

silver nanospheres orients along the electric field of a linearly polarized trapping laser. Therefore, it can stably spin in the plane perpendicular to the trapping laser propagation direction if the polarization direction rotates. They developed a method to obtain the interparticle distance and the azimuthal angle of the dimer with an accuracy of a few degrees independent of the wavelength or the distance between the interacting nanoparticles. In this way, they could explore the effect of spinning speed on the interparticle distance of the PNPs dimer.

Dimers can be also exploited as sensors of the dynamics and interactions of PNPs in an optical trap[61]. J. A. Rodrigo et al.[62] achieved the controlled transport of multiple silver PNPs within a freestyle optical trap (structured single-beam trap shaped as a diffraction-limited arbitrary curve). They could detect regions of slower motion of the PNPs along the freestyle optical trap path due to the formation of dimers when PNPs circulating through the trap approached each other as they experienced less propulsion in those regions. They directly observed the formation of dimers in real time by means of a CCD camera (Fig. 2(g)). They observed that PNPs dimers move on average 2.8 times faster than single PNPs. This is due to the large extinction cross-section of the dimers (2.6 times larger than for the monomer), which therefore should experience an optical propulsion force about 2.6 times stronger than a single PNP.

Furthermore, as the plasmon resonance wavelength of a dimer is highly sensitive to the separation among the interacting PNPs, dimers are therefore also called plasmonic rulers[63,64]. F. Han et al.[64] optically trapped a core-satellite plasmonic system joined by a thermo-responsive polymer (Fig. 2(h)). They modified the heating achieved by the trapped plasmonic system by varying the applied trapping laser power. Then, when the collapse temperature (T_c) of the thermo-responsive polymer was reached, the system underwent the irreversible approach of the core and the satellites PNPs, which coupled experiencing a shift of their plasmon resonance wavelength. However, some core-satellite plasmonic systems tended to disassociate into the constituent gold PNPs when irradiated at large laser powers. The authors attributed that to the instability of the thiol bond used to join the thermo-responsive polymer to the PNPs.

Lanthanide-doped nanoparticles

The specific electronic configuration of lanthanide-doped nanoparticles leads to narrow emission bands and long lifetimes, typically between micro- and milliseconds. Fluoride-based crystalline matrices are being more frequently used as hosts because fluorides are characterized by low-energy phonons. Consequently, the number of phonons required to depopulate the excited energy levels of Ln^{3+} ions is larger than in other hosts and so the probability of non-radiative decays is minimized. Among Ln^{3+} doped fluoride nanocrystals, Er^{3+}-Yb^{3+} co-doped ONPs (so-called upconverting nanoparticles, UCNPs) have attracted special attention due to their ability to convert infrared radiation into visible and ultraviolet (UV) emission. This allows to excite UCNPs in the infrared biological transparency windows for deep tissue imaging[65]. Moreover, they can be excited using low power and inexpensive near-infrared (NIR) lasers and their luminescence can be detected with cost-effective silicon detectors[66]. Optical trapping of UCNPs was firstly demonstrated by P. Haro et al., where dielectric $NaYF_4$:Er^{3+},Yb^{3+} nanoparticles were trapped and excited using a 980 nm single-laser beam[67]. As shown in Eq. (1), the optical force experienced by ONP is determined by their electronic polarizability. For dielectric nanoparticles, as lanthanide-doped nanoparticles, the polarizability is defined as[34]:

$$\alpha' = 4\pi r^3 \frac{{n_{\rm NP}}^2 - {n_{\rm m}}^2}{{n_{\rm NP}}^2 + 2{n_{\rm m}}^2}\,, \tag{2}$$

where r and $n_{\rm NP}$ are the radius and the refractive index of the trapped nanoparticle, respectively, and $n_{\rm m}$ is the refractive index of the surrounding medium. As polarizability is proportional to r^3, typical UCNPs undergo trapping forces of femtonewtons. Although these forces can be used to trap particles, they may be too weak for applications in viscous media such as intracellular controlled trapping. Thus, an enhancement of optical forces is needed. As an increase in trapping beam intensity can damage the cells by heating and an increase in particle size can reduce the ability of UCNPs to be internalized in living cells, innovative strategies have been developed. First, polarizability can be optimized by increasing α through UCNPs surface modification. The effect of a coating covering a nanoparticle on the electronic polarizability is given by[34]:

$$\alpha' = 4\pi r^3 \frac{(\varepsilon_2 - \varepsilon_{\rm m})(\varepsilon_1 + 2\varepsilon_2) + f(\varepsilon_1 - \varepsilon_2)(\varepsilon_{\rm m} + 2\varepsilon_2)}{(\varepsilon_2 + 2\varepsilon_{\rm m})(\varepsilon_1 + 2\varepsilon_2) + f(\varepsilon_1 - \varepsilon_2)(2\varepsilon_2 - 2\varepsilon_{\rm m})}\,, \tag{3}$$

where ε_1 and ε_2 are the permittivity of the nanoparticle and the coating, respectively. A suitable coating leads to

an increment of α and, consequently, an enhancement of the optical force. This strategy has been used by several authors to easily manipulate UCNPs[33,34]. An enhancement of optical forces can also be achieved by increasing the doping of lanthanide ions. X. Shan et al.[68] found that highly doped UCNPs can generate a strong oscillation resonance effect in the electromagnetic field, resulting in a significant enhancement of the optical trapping force. Both strategies are essential for 3D controlled optical trapping of UCNPs, allowing simultaneously imaging and sensing.

Thermal sensing with an optically trapped lanthanide-doped nanoparticle

In addition to the above-described properties, UCNPs are also sensitive to temperature. Such ability is based on the specific energy level diagram of UCNPs (Fig. 3(a))[69]. After excitation of Yb^{3+} with infrared (980 nm) radiation, energy is transferred to Er^{3+}. Subsequent absorption of 980 nm photons from excited states of Er^{3+} ions populate their high energy $^4F_{7/2}$ level from which both $^4S_{3/2}$ and $^2H_{11/2}$ states are populated. Radiative de-excitation from these states to the ground level are responsible for the green emission bands at 520 and 540 nm ($^2H_{11/2}\rightarrow{}^4I_{15/2}$ and $^4S_{3/2}\rightarrow{}^4I_{15/2}$, respectively). These two states are so close in energy that they are thermally coupled, i.e., their relative populations follow the Boltzmann statistics. Consequently, the temperature dependence of relative intensities of the emissions generated at 520 and 540 nm makes determining temperature possible from a ratiometric analysis of the emission generated by Er^{3+}-Yb^{3+} co-doped UCNPs[66,70–75]. Indeed,

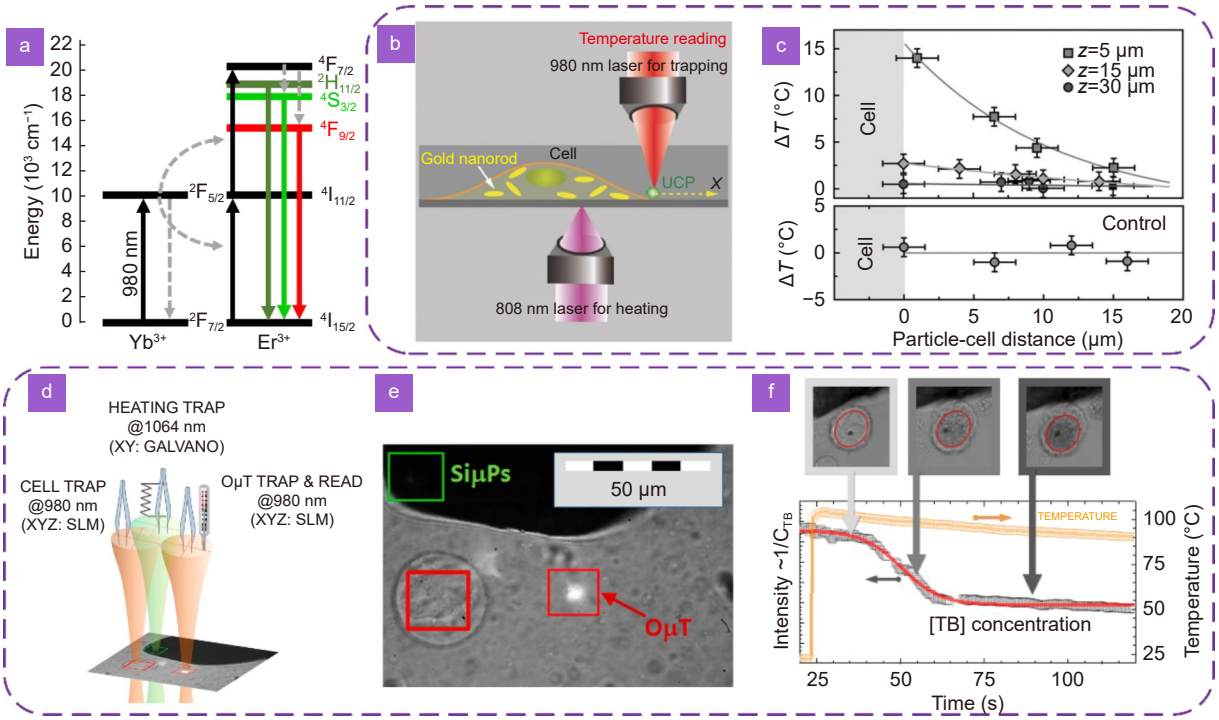

Fig. 3 | Lanthanide-doped nanoparticles for thermal sensing. (**a**) Energy scheme of Er^{3+}-Yb^{3+} co-doped UCNP. Black continuous arrows indicate $^4F_{7/2}$ level population by an energy transfer process. Grey discontinuous arrows indicate energy transfer processes between Er^{3+} and Yb^{3+} ions. Dark green ($^2H_{11/2}\rightarrow{}^4I_{15/2}$), light green ($^4S_{3/2}\rightarrow{}^4I_{15/2}$), and red ($^4F_{9/2}\rightarrow{}^4I_{15/2}$) continuous arrows indicate radiative emissions centered at 520 nm, 540 nm, and 660 nm, respectively. (**b**) Schematic representation of the experimental setup used for thermal scanning in the surroundings of a HeLa cell subjected to a plasmonic photothermal treatment. The arrow indicates the scanning direction. (**c**) On the top, the temperature decay measured from cell surface for three different distances from the substrate. The symbols are the experimental data, and the lines are a guide for the eyes. On the bottom, the control experiment in absence of the 800 nm heating laser. (**d**) Functional scheme of the active dual-wavelength optical multitrap setup. The 980 nm beams (orange cones) for trapping of the cell and trapping/reading of the optical microthermometers, while the 1064 nm optical trap (green cone) for optical trapping/heating. (**e**) Microscope image of the cell, silica microparticles and optical microthermometers being trapped, activated, and read. Red rectangles represent 980 nm trapping laser, while green rectangles represent 1064 nm trapping laser. (**f**) Time lapse images of the heated cells at 10, 30, and 65 s after switching on the heating. On the bottom-right, graphs of relative Trypan Blue (TB) accumulation in the dying cell and the corresponding temperature (right axis). Figure reproduced with permission from: (b, c) ref.[14], Copyright 2016 John Wiley and Sons; (d–f) ref.[80], Copyright 2017 American Chemical Society.

$NaYF_4$:Er^{3+},Yb^{3+} UCNPs are the most commonly used lanthanide-doped nanothermometers because of their superior luminescence brightness, good chemical and physical stability, and low toxicity[66,76–79].

Thermal sensing from a single UCNP requires simultaneous trapping and emission acquisition. This becomes feasible since one of the most common fiber-coupled lasers used for trapping works at 980 nm, so it can be used for simultaneous excitation of UCNPs. As it is mentioned in Section *Lanthanide-doped nanoparticles*, the main challenge is the low optical forces typically acting on UCNPs. Indeed, long term trapping of a single UCNP is not easy. Therefore, it is not surprising that the first demonstration of simultaneous trapping and thermal sensing was demonstrated in Er^{3+}-Yb^{3+} co-doped upconverting microparticles (UCMPs). P. Rodríguez-Sevilla et al.[14] have used $NaYF_4$:Er^{3+},Yb^{3+} UCMPs to determine the thermal gradient induced in the surrounding of a live cancer cell being subjected to a photothermal therapy. In their experiments, authors favoured cell heating by incorporating gold nanorods and exciting them with an 800 nm laser focused within the treated cell. As it is mentioned in Section *Plasmonic nanoparticles*, since gold nanorods are PNPs, they have a high light-to-heat conversion efficiency. The 800 nm laser was used as a light source to induce heat generation process. The heat generated will gradually diffuse into the cancer cell. For the estimation of the thermal gradient in the surroundings of a cancer cell, $NaYF_4$:Er^{3+}, Yb^{3+} UCMPs were added to the cell culture medium. A second 980 nm laser focused within the culture medium was used to trap and excite a single $NaYF_4$:Er^{3+},Yb^{3+} UCMP (Fig. 3(b)). Translation of the 980 nm laser beam allowed to scan the upconverting particle away from the cell while performing continuous acquisition of emission spectra, i.e., simultaneous thermal sensing. Figure 3(c) shows the temperature gradient at different horizontal distances from the cells obtained at three different heights. In this figure, the temperature profile obtained in a control experiment (800 nm laser beam was switched off) is also included revealing a complete absence of heating. From experimental data, author concluded that during photothermal treatment of individual cells the thermal gradient created in the surroundings extends over 10 μm, affecting surrounding cells and hindering single-cell treatments.

In 2017, S. Drobczyński et al.[80] also scanned the thermal gradient in the vicinity of the diffuse large B-cell lymphoma (DLBCL) cells due to locally induced hyperthermia. In this case authors used optical microthermometers (OμTs) fabricated by encapsulating $NaYF_4$:Er^{3+}, Yb^{3+} UCNPs with amorphous silica shells of about 6 μm in diameter. For heating, mesoporous silicon microparticles (SiμPs) were used. DLBCL cells, microthermometers, and SiμPs particles could be simultaneously trapped by an active dual-wavelength optical multitrap (Fig. 3(d)), where two different 980 nm laser beams (orange cones) were used to trap the DLBCL cells and OμTs and a 1064 nm laser beam (green cone) is used to trap the SiμPs particles, simultaneously converting light into heat. To quantify the damage to the cells due to temperature increase, the accumulation of Trypan Blue (TB) inside the cells was simultaneously measured. Optical microscope imaging was used to locate the OμTs close to the cells for thermal reading (Fig. 3(e)). As it is shown in Fig. 3(f), the temperature in the cells environment increases up to almost 100 °C, thermally injuring them. That is also manifested by a TB accumulation in the damaged cells 15 seconds after the temperature rise. It took another 15 seconds to reach TB saturation in the damaged cells, so the damaged cells respond attempting to alleviate the damage provoked by heating.

Intracellular viscosity sensing with an optically trapped lanthanide-doped nanoparticle

Intracellular viscosity is an essential parameter that plays a crucial role in the diffusion in biosystems[81]. It is strongly related with the mechanical deformability of the cytoplasm[82]. In turn, this affects many cellular and subcellular processes such as the translocation of organelles, partially controlled by their frictional drag and consequently by the viscoelastic properties of the cytoplasm[83–86]. At cellular level, viscosity is also critical for protein–protein interactions and transportation of small solutes, macromolecules, and other cellular organelles in living cells[87]. Thus, changes in intracellular viscosity are associated to different diseases, as diabetes[88], atherosclerosis[89], and Alzheimer's disease[90].

Besides the superior luminescent properties of $NaYF_4$:Er^{3+},Yb^{3+}, the non-centrosymmetric crystalline phase causes the luminescence to be polarized[91–94]. The spectral shape of both green and red bands depends on the propagating direction and polarization of detected emission. The emission spectra can be explained in terms of three main polarization states: σ (light propagating along the optical axis (z-axis) with a polarization perpendicular to it (parallel to x- or y-axes)), α, and π (light

propagates perpendicularly to the optical axis of the UCNP with a polarization perpendicular (α) or parallel (π) to it) (Fig. 4(a)). Figure 4(b) shows, as an example, the red emission generated by a $NaYF_4$:Er^{3+},Yb^{3+} UCNPs as obtained in each of these states[15]. Once the emission spectra corresponding to each of these configurations is known, it is possible to determine the orientation of an UCNP by just analysing their spectral shape[92,95]. Not only that, but a real time analysis of emission spectra also generated by UCNPs can be used to determine the rotation velocity of the particle while rotating from its initial position (optical axis parallel to the propagation direction of laser beam) to its steady state position (optical axis perpendicular to the propagation direction of laser beam). For a fixed torque (fixed laser trapping power) the rotation velocity depends on the medium viscosity, so that the analysis of the emission spectra can be used to determine the medium viscosity. This possibility was explored by P. Rodriguez et al. using submicrometric $NaYF_4$:Er^{3+},Yb^{3+} particles within HeLa cells (Fig. 4(c))[15]. An analysis of the polarization state of the red emission of Er^{3+} ions allowed the authors to access to the orientation of the particle within the cell as well as its rotation velocity (w_l, what authors called active determination of intracellular viscosity.) The intracellular viscosity was obtained from the angular velocity of the particle by just applying:

$$\eta_{\text{cell}} = 6.7 \times 10^{-14} \times I_{\text{L}} \frac{2\pi}{w_l}\,, \tag{4}$$

where I_{L} is the laser intensity. Additionally, intracellular viscosity was also determined from the oscillations of the trapped particle around its stable position. This is what authors named passive method, where the mean square angular displacement of the particle in the trap ($MSAD$) is analysed as a function of the lag time (τ). The intracellular viscosity is then given by:

$$\eta_{\text{cell}} = \frac{RT}{3 \cdot MSAD \cdot V_{\text{p}} \cdot f/f_0}\tau^{\alpha}\,, \tag{5}$$

where f/f_0 is the Perrin friction factor for the trapped particle defined by the friction factor of the particle (f) and the friction factor of a spherical body (f_0), R is the ideal gas constant, T represents the temperature of the medium, V_{p} stands for the volume of the particle, and α

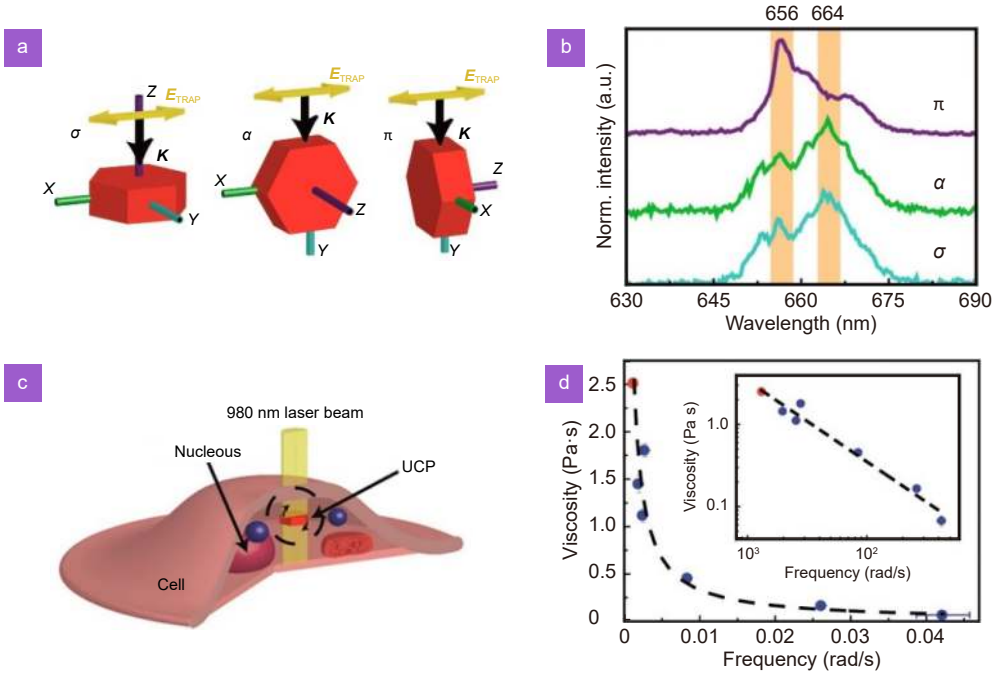

Fig. 4 | Lanthanide-doped particles for intracellular viscosity sensing. (**a**) Diagram of the three excitation configurations. σ-polarization state, defined by propagating light along the optical axis (*z*-axis) with a polarization perpendicular to it (parallel to *x*- or *y*-axes) and *α*- and π-polarization states, where light propagates perpendicularly to the optical axis of the UCNP with a polarization parallel (π) or perpendicular (*α*) to it. (**b**) Emission spectra along the three polarization states. (**c**) Schematic representation of the rotation of a UCNP inside a HeLa cell. (**d**) Measured viscosity as a function of the rotation frequency. Inset is the log−log representation. Blue data correspond to the values measured by the active method while red data is the averaged value obtained from passive method experiments. The rotation frequency for passive method is estimated by dividing the accumulated rotated angle by the elapsed drag. Black dashed lines correspond to the best fitting. Figure reproduced with permission from ref.[15], Copyright 2016 American Chemical Society.

determines if the movement of the particle is restricted ($\alpha < 1$) or if it experiences superdiffussion ($\alpha > 1$) (in this case, they set $\alpha = 1$). As it can be observed in Fig. 4(d), a good agreement between both methods was obtained. Furthermore, authors were able to measure both the static and dynamic intracellular viscosity. They could also determine how the intracellular viscosity varies with the rotation frequency, as it can be expected from Eq. (4). A mean static value of 2.51 Pa·s has been obtained for the static viscosity in the cytoplasm, which is very close to the value obtained (2.3 Pa·s) by S. Chakraborty et al.[96], who used fluorescence correlation spectroscopy measurements of gold nanocluster, to determine its diffusion time in HeLa cells. Both experimental results are similar to the one obtained by analysing the movement of fluorescence magnetic nanoparticles inside the cells under a local field (1.45 Pa·s), method developed by I. Ramazanova et al.[97]

Chemical sensing with an optically trapped lanthanide-doped nanoparticle

Adequate surface functionalization of upconverting particles can convert them into chemical sensors, in particular of pH. First UCNPs pH-sensors were obtained by coating $NaYF_4$:Er^{3+},Yb^{3+} with polyglutamic porphyrin-dendrimers[16]. The energy transfer from the UCNP to the porphyrin chromophore exhibits a pH-dependent absorption at 660 nm, leading to a decrease of the red luminescence emission of the UCNP with decreasing pH and so, to a pH-dependent red-to-green emission ratio[98]. First demonstration of pH sensing based on a single UCMP was published by K. Suresh et al.[17] In their pioneering work authors demonstrated how an optically trapped polyethyleneimine capped UCMP can act as a broad range pH probe. With this specific coating, the ratio between red and green emissions of Er^{3+} ions becomes strongly pH-dependent. The ratio between red and green emissions of a trapped UCMP shows a linear dependence on pH values (Fig. 5(a)). This behaviour was confirmed using different buffer solutions (Fig. 5(b)). Nevertheless, it must be considered that the emission ratio is different for each buffer solution, thus this pH probe is not independent on the composition of the surrounding medium. In conclusion, the authors have developed a robust reproducible pH sensor, based on red to green emission ratio analysis of a single UCMP trapped in a microchannel, even though it must be calibrated for each medium to be measured.

Fluorescent polymeric nanoparticles

Dielectric particles like polymeric particles are widely used in OTs experiments since they are commercially available. An advantage of polymeric particles is their higher refractive index at NIR wavelengths, which enhances optical forces and therefore facilitates more stable optical manipulation in water. However, pure polymeric nanoparticles are non-luminescent, so visualizing them within the trap is challenging. Incorporation of dyes into the polymeric nanoparticles is an easy way to make them luminescent and easy to track within the optical trap. As it is explained in next sections, the tracking of the polymeric nanoparticles makes it possible to study single particle dynamics and develop biological applications.

Investigation of single particle dynamics by optically trapped polymeric nanoparticles

There have been some reports on the dynamics of microparticles in optical traps[99,100]. For ONPs application in

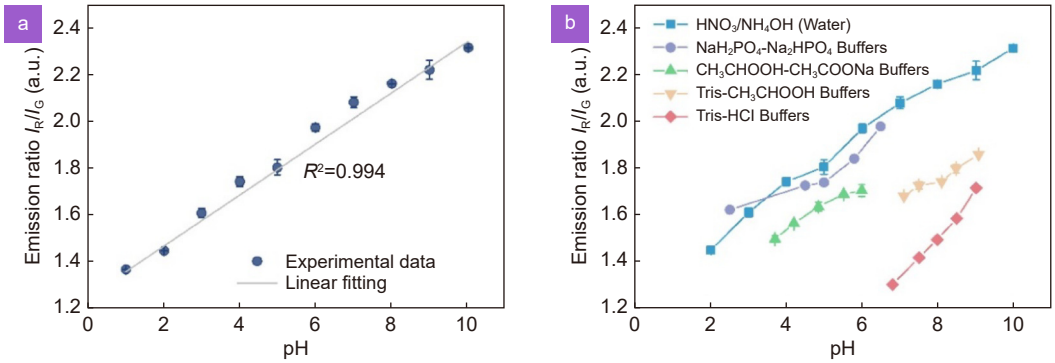

Fig. 5 | Lanthanide-doped particles for chemical sensing. (**a**) Red to green emission ratio depending on pH value for a single UCMP in a buffer solution. Blue dots are experimental data. Grey line is the linear fitting. (**b**) Red to green emission ratio of the optically trapped UCMP vs. pH in various buffer solutions. Figure reproduced with permission from ref.[17], under a Creative Commons Attribution 3.0 International License.

aqueous environment, it is also essential to understand the dynamic process of a nanoparticle stepping into an optical trap. The visualization of ONPs facilitates the study of dynamics at the nanoscale.

The effect of their own luminescence on the optical trapping forces is of high interest. R. Bresolí-Obach et al.[101] studied the optical resonance effect (ORE) between a single dye-labeled polystyrene nanoparticle and the trapping laser. A 1064 nm laser was used for trapping, and a 488 nm laser was used for dye excitation. They found a 4-fold trapping stiffness enhancement due to resonant excitation under 488 nm irradiation. As shown in Fig. 6(a), upon 488 nm excitation, S_1 was populated, and the 1064 nm laser was cyclically resonant with the S_1–S_2 excited state electronic transition. The 1064 nm photons absorption in the S_1–S_2–S_1 cycle enhanced the polarizability of the system, leading to an increase in the induced radiation force that was responsible for the observed ORE. Theoretical calculations in Fig. 6(b) indicate the increasing $S_1(v_0)$ and $S_2(v_0)$ state population for resonance. When the 488 nm excitation was off (Fig. 6(c)) or the particle was labeled with fully photobleached dye (Fig. 6(d)), the trapping stiffness enhancement was no longer observed.

In order to study how a particle incorporates to the circularly polarized laser trap, B. Louis et al.[102] directly mapped the 3D incoming trajectory of NPs toward a stable optical trapping spot using a 200 nm fluorescent polystyrene particle. As shown in Fig. 7(a), they used a widefield multiplane microscope to achieve multiplane fluorescence imaging. The particles followed a Brownian motion outside the irradiated area and then exhibited a helicoidal motion once they entered the "trapping region" (Fig. 7(b)). The shallow cone shape incorporation of most of the ONPs in OT was observed (blue lines). However, not all the ONPs followed the same shallow cone trajectory. There were some ONPs that happened to be trapped for a short time in a metastable position around 2 μm below micrometers below the optical trapping focus before they were pushed to the focal spot (red

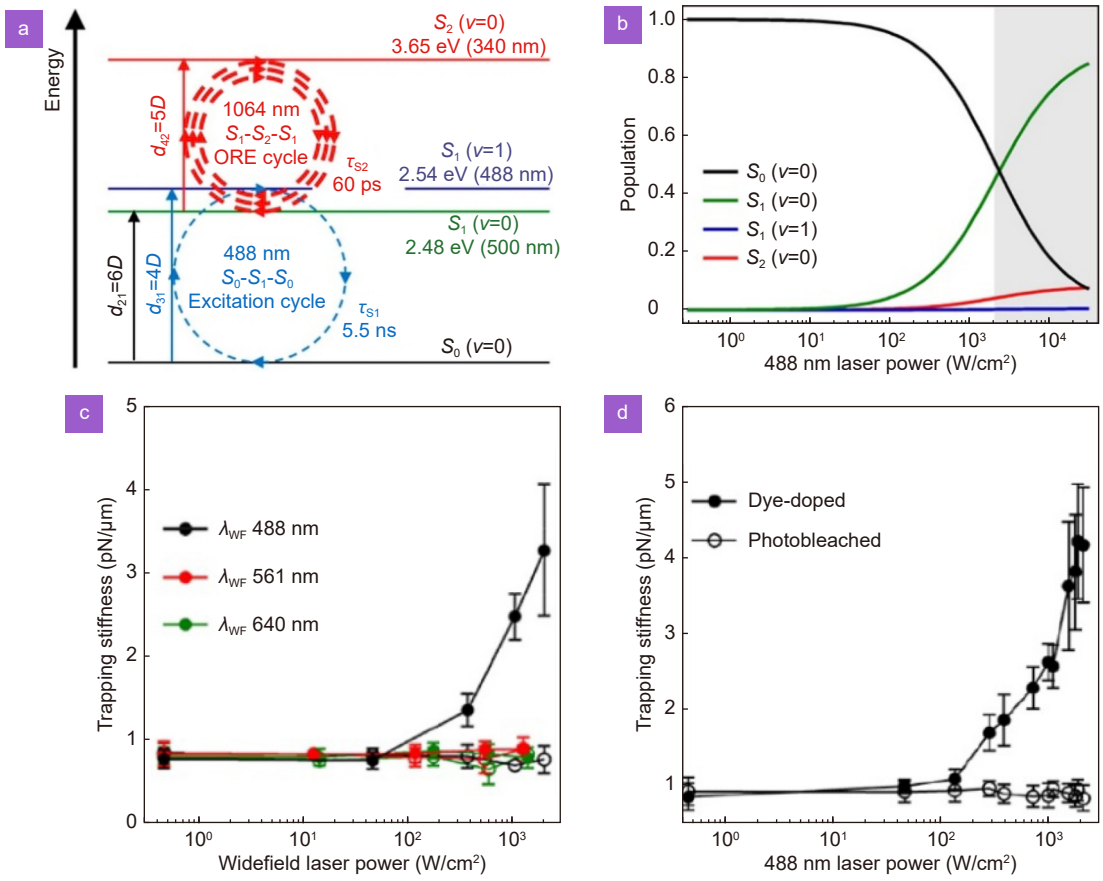

Fig. 6 | (**a**) Jablonsky diagram of the electronic states involved in the optical resonance effect. (**b**) Theoretical calculations of the population of each state vs the 488 nm excitation power. (**c**) Changes in the trapping stiffness vs the excitation wavelength, there is no fluorescence or resonance effect without 488 nm excitation. (**d**) Changes in the trapping stiffness vs the 488 nm laser power. Figure reproduced with permission from ref.[101]. Copyright 2021 American Chemical Society.

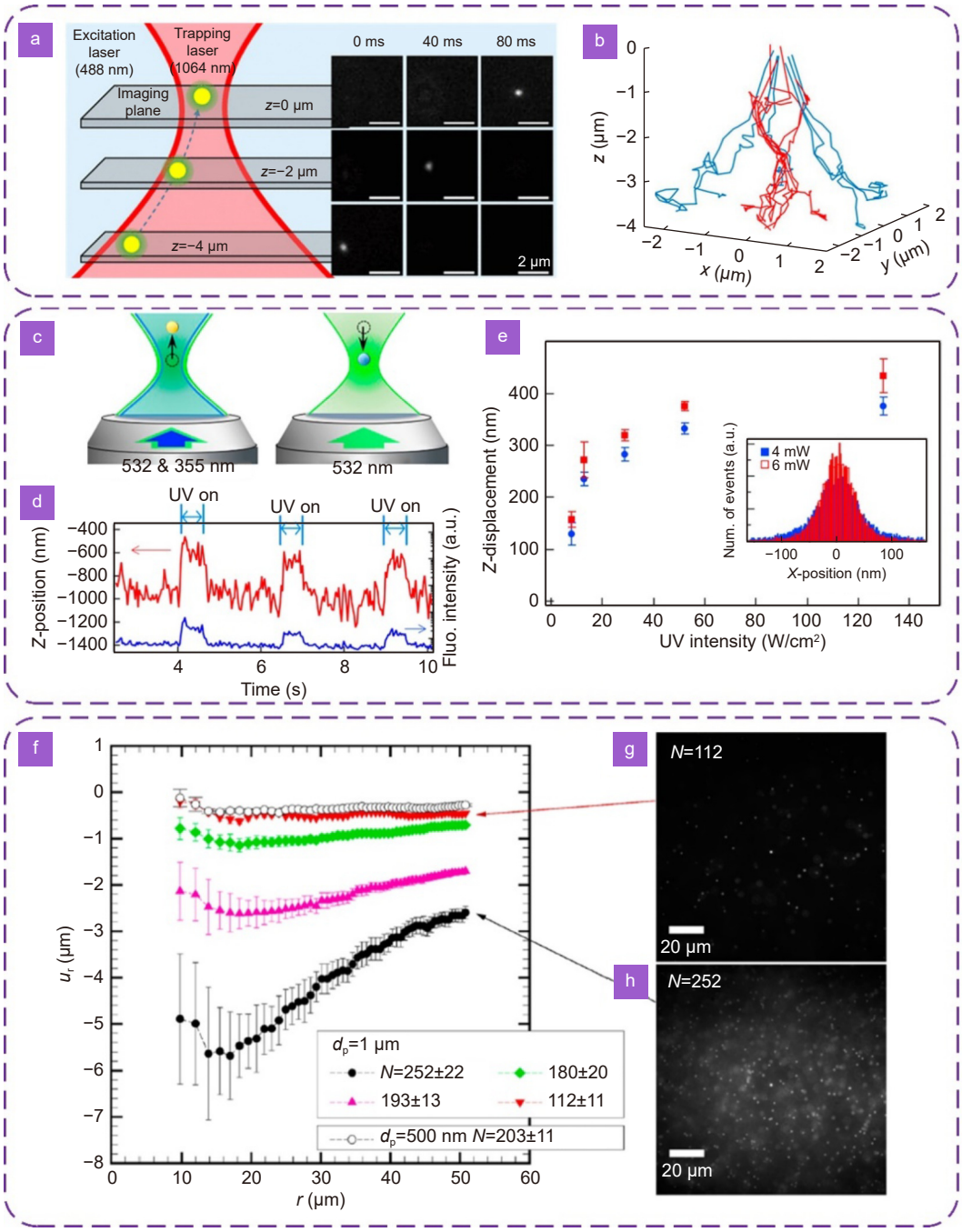

Fig. 7 | Fluorescent polymeric particles for investigation of single particle dynamics. (**a**) Left: Schematic of multiplane microscope with optical tweezer. Right: Time frame of fluorescent images from different planes. (**b**) 3D incorporation trajectories of 200 nm fluorescent polystyrene particles in an optical trap. Blue and red lines represent the incorporation trajectories going through the inner and outer cones, respectively. (**c**) Schematic of mesoscopic mechanical motions induced by the photochromic reaction of a single PMMA particle. (**d**) Time course of the positional change along the *Z* axis (red line) and the fluorescence intensity (blue line) of a trapped particle with the continuous wave 532 nm laser. (**e**) Z displacement of a fluorescent particle under trapping. (**f**) Profile of radial flow component u_r for various particle numbers (*N*) and diameters (d_p). (**g**–**h**) Snapshots of the fluorescence images of different numbers of 1 μm polystyrene particles around the optical trap. Figure reproduced with permission from: (a, b) ref.[102], under a Creative Commons Attribution 4.0 International License; (c–e) ref.[103], Copyright 2023 American Chemical Society; (g–h) ref.[104], Copyright 2020 American Chemical Society.

lines). This metastable position indicates that there is a secondary focal point around 2 μm below the main focal point. It is induced by the interference of the focusing beam. The author confirmed the existence of secondary focal point by the calculated electric field intensity distribution. S. Ito et al.[103] demonstrated the photoswitching of radiation forces acting on a particle by using photochromic reactions of fluorescent diarylethene derivative (DE1). DE1 was put into 300 nm PMMA (poly(methylmethacrylate)) particles by swelling method. Photochromic reaction was controlled by UV irradiation, as Fig. 7(c) illustrates. The vertical Z position of a trapped particle was dependent on the scattering, absorption, and gradient forces. The scattering and absorption forces were proven to be affected by dramatical photochromic reaction, thus leading to the Z displacement of the particle (Fig. 7(d, e)).

OTs are usually employed in flow conditions. C. Hosokawa et al.[104] revealed the fluid flow in an OT by particle-image-velocimetry of fluorescent polymeric particles. They proposed a new mechanism based on the ability of scattering force to alter the fluid dynamics through the interaction with the laser-induced particle motion. Authors were even capable of distinguishing the relevance of particle number and size in the process. To demonstrate it, they recorded the fluorescence images of 500 nm and 1 μm fluorescent polystyrene particles around optical traps every few seconds. The radial component of flow vector u_r was analyzed (Fig. 7(f)). The case of 500 nm nanoparticles exhibited significant smaller flow speed compared with the case of 1 μm ones. Moreover, for the 1 μm nanoparticles, the increasing number of particles increased the flow speed (Fig. 7(g, h)). It denied the conventional thermal convection, which is independent of sizes and number of particles. Instead, they found that the fluid dynamics result from the direct impact of the optical forces acting on the suspended particles. Authors also found that the optical force and the resulting particle motion can be used to induce the large-scale fluid convection to accumulate the particles to the laser focal spot.

These works show us the dynamic motion of single or multiple ONPs in an optical trap in a visual way. They facilitate a more thorough comprehension of optical and mechanical interaction between trapping laser and optical particles. The measurement errors that may arise from such dynamics need to be considered during the practical application of optically trapped ONPs.

Optical trapping of polymeric nanoparticles for bioapplications

There are some attempts of using optically trapped polymeric nanoparticles for the study and characterization of biological samples. It was proposed in 1996 by E. L. Florin et al.[105] Authors demonstrated the potential application of fluorescent latex beads for topological imaging of biological systems. In 1997, they used an optically trapped 200 nm fluorescent latex bead as a sensing unit for scanning probe microscopy[106]. When the trapping laser was fixed vertically and scanned horizontally, the intensity of the fluorescent signal varied because the particles were displaced away from the trapping laser focus when scanning the surface of the bio-object (Fig. 8(a)). Therefore, the intensity of the fluorescence emission from latex bead depended on its displacement. This feature was utilized to reconstruct a map of the height of the bio-object. In particular, the authors demonstrated how a two-dimensional image can be formed by laterally scanning the trapped latex bead across biological samples while recording the two-photon-induced fluorescence intensity. They successfully obtained a scanning image of the outer surface of a small neurite from a cultured rat hippocampal neuron and converted it to a height profile.

Later, M. J. Lang et al.[107] developed an instrument combining OTs and single-molecule fluorescence. They used a 500 nm optically trapped dye-labeled polystyrene bead as the mechanical load to separate the strands of individual DNA molecules labeled with fluorescent dyes. A DNA duplex with an overhanging segment was attached at one end to a polystyrene bead. Its distal end was annealed at to a 15 base-pair oligonucleotide, anchored directly to the glass surface. Tetramethylrhodamine dyes conjugated to nucleotides were placed on complementary bases, one on the 3-end of the shorter 15-mer and the other on the 5-end of the long strand (Fig. 8(b)). Quenching of fluorescence happened due to the proximity of dye. The DNA-bead complex was trapped, and the microscope stage was moved at constant velocity to pull the bead from the center of the trap, which increased the load until rupture. Both rupture-force and fluorescence were monitored simultaneously. The rupture-force was converted from bead displacement from the trap center. The rupture of DNA molecules was monitored thorough the intensity of dye fluorescence. Before rupture the dye was quenched. However, upon rupture the fluorescence level increased abruptly as the two fluorophores were separated. This dye photobleached in several seconds

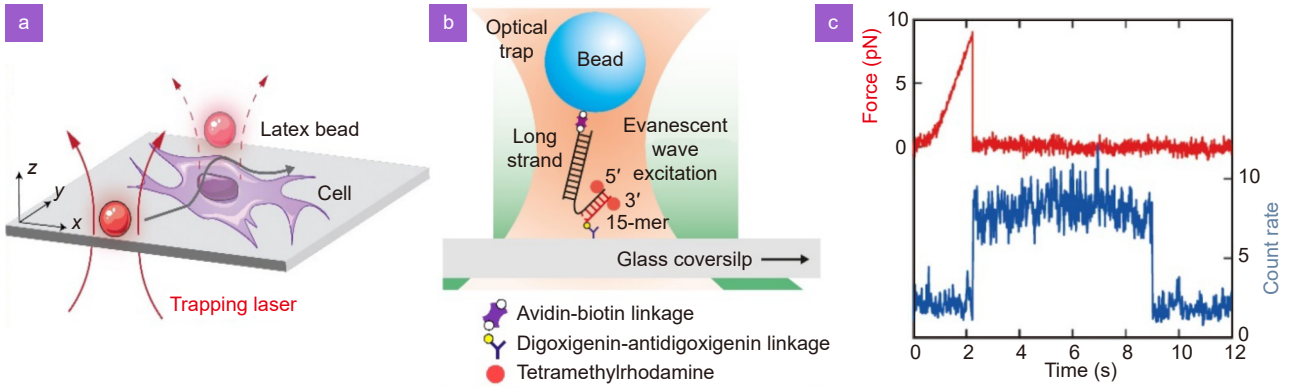

Fig. 8 | Fluorescent polymeric particles for biological applications. (**a**) Scheme of the scanning procedure: a latex bead is trapped by the focused laser beam (red arrows). The fluorophore in the latex beads is excited by laser light via a two-photon absorption process. When the trapped bead is moved across an obstacle such as a cell (grey arrow), it is pushed out of the laser focus and the fluorescence intensity decreases. (**b**) A 500 nm polystyrene bead is tethered to cover glass surface by a 1010 base-pair DNA molecule, consisting of a long strand (black) joined to a shorter 15- base-pair duplex region (red). (**c**) Simultaneous records of force (red trace) and fluorescence (blue trace). Rupture occurred at 2 s at an unzipping force of 9 pN. The dye unquenched at the point of rupture, and later bleached at 9 s. Figure reproduced with permission from: (b, c) ref.[107], under a Creative Commons Attribution 4.0 International License.

and the light signal returned to background level (Fig. 8(c)). These results demonstrated the instrument capable of studying single molecule structure and mechanics. They successfully applied this method to measure the force needed to unzip or shear duplex DNA molecules[108].

In summary, as polymeric nanoparticles have been widely used for bioimaging and theragnostic, the combination of optical trapping of polymeric nanoparticles with fluorescence microscopy or scanning probe microscopy are promising strategies to broaden their application.

Semiconductor nanoparticles

Semiconductor quantum dots (QDs), nanorods, and nanowires have recently gained great attention thanks to their special photoluminescence properties such as tunable emission, lower susceptibility to photobleaching, high quantum yields, and chemical stability. Semiconductor nanoparticles are widely used in biomedicine as molecular sensors[109–111] and photostable substitutes for fluorophores in bioimaging[112]. The potential application of semiconductor nanoparticles can be even expanded if they can be isolated and manipulated individually by optical traps, as later described in this section. Optical trapping of individual semiconductor nanocrystals was demonstrated for the first time in 2007 by L. Y. Pan et al.[113], who gave some hints to make trapping easier such as to work on D_2O medium to prevent the thermal increase of Brownian motion and therefore increase the trapping stability. This pioneering work motivated other researchers to work on the optical trapping of QDs for different purposes and in different experimental conditionsl conditions[114–118]. As it has been described for birefringent upconverting particles, simultaneous trapping and rotation of no-spherical semiconductor nanocrystals was also possible as demonstrated by C. R. Head et al.[119] Optical trapping of semiconductor nanocrystals has been also used for the fabrication of complex structures[120]. Among the experimental demonstrations of optical trapping of semiconductor nanocrystals in this review, we summarize and highlight those works in which the optical response of the trapped semiconductor nanoparticle is of relevance, such as those studying single particle spectroscopy or achieving cell imaging.

Optical trapping of semiconductor nanocrystals for single particle spectroscopy

Before applying the semiconductor nanocrystals to in vitro applications, it is essential to understand and improve the luminescent properties of single particles or small clusters. P. Pinapati et al.[121] proposed the trapping of 35 nm silica-shelled quantum dots on graphene oxide (GO) to study the quenching behavior of QDs. They achieved the first optical trapping of QDs at low intensities, on the order of few $\mu W/\mu m^2$, in the presence of GO. The emission quenching of the QD@SiO_2 trapped on GO was studied (Fig. 9(a)). As shown in Fig. 9(b), the emission of the trapped QD@SiO_2 remained unquenched for 120 s in the absence of GO. This strong quenching behavior has been attributed to a nonradiative energy transfer mechanism from the QD to the GO.

Photobleaching may hinder the use of semiconductor nanoparticles in OTs. To tackle that problem, H. Rodríguez-Rodríguez et al.[122] demonstrated the photobrightening and bleaching dynamics of optically trapped silica encapsulated QDs clusters. They studied two types of silica-encapsulated quantum dots excited upon two-photon absorption in an optical trap. The first type consists of alloyed CdSeZnS quantum dots were covered with a silica shell (QD@SiO_2). The second type had an extra intermediate sulfur passivating shell (pQD@SiO_2). Both tolerated irradiance doses 3 orders of magnitude higher than those reported for bare core/shell architectures. Meanwhile, the extra sulfur layer allowed a more gradual intensity decrease under continuous irradiation. They concluded that the sulfur layer can provide better passivation, suppress bleaching, and enable higher luminescence stability (Fig. 9(c, d)).

Optical trapping of semiconductor nanocrystals for cell imaging

Optically trapped semiconductor nanocrystals can act as energy converters for local in vitro fluorescence activation. P. J. Pauzauskie et al.[123] demonstrated the possibility to scan a cylindrical GaN nanowire across the cell membrane into living Hela cell by optical trapping. The position of GaN nanowire could be manipulated and maintained for arbitrary time. They chose a 1064 nm trapping wavelength because the cells can tolerate limited infrared laser. GaN emitted ultraviolet light under the two-photonexcitation by the trapping laser. In this way, GaN nanowire could act as a local subwavelength ultraviolet nanolaser to excite local fluorophores for precisely positioned cellular imaging. The feasibility of nanowires as local point-like illumination source was further demonstrated by Y. Nakayama et al.[124]. The emission from an optically trapped $KNbO_3$ nanowire was used to excite the two-photon absorption of a fluorescent dyed polystyrene bead in near field. H. Rodríguez-Rodríguez et al.[125] also used optically trapped QDs as localized emitters to induce photoluminescence of dye-labeled cells. As shown in Fig. 10(a), the silica-coated colloidal QDs were simultaneously excited and manipulated

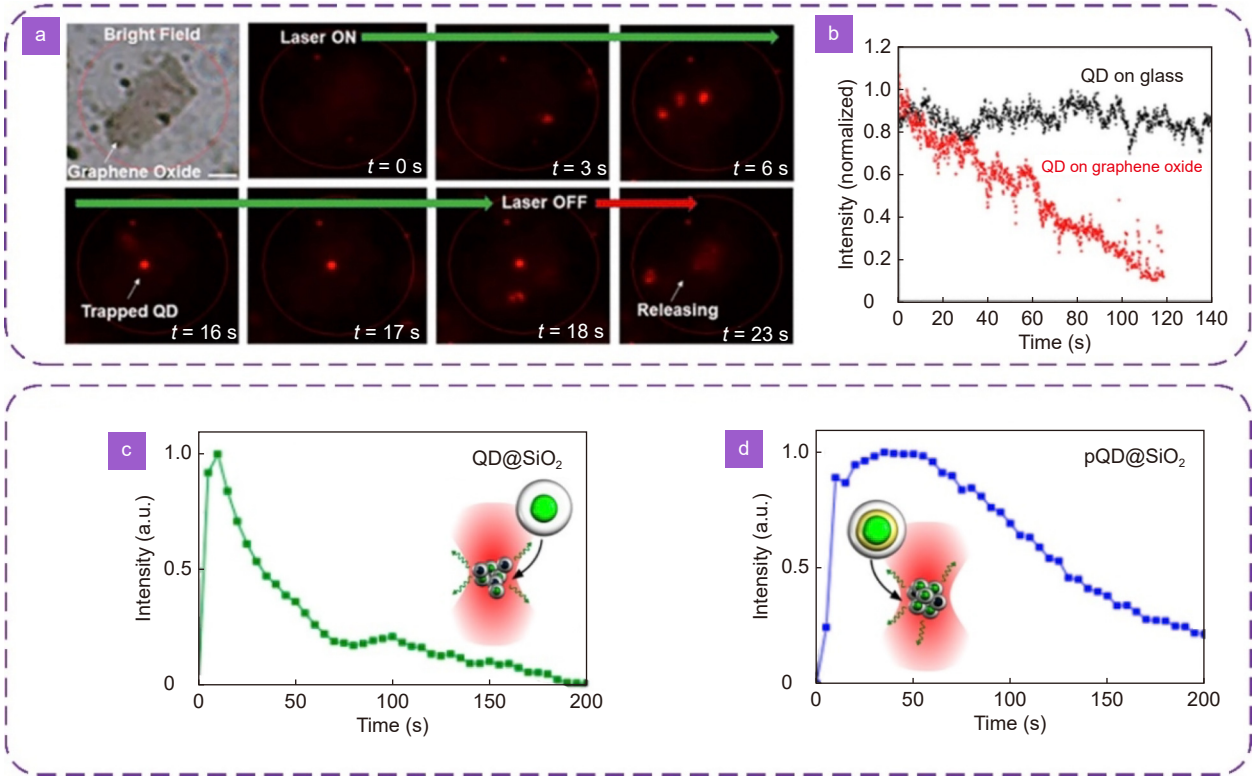

Fig. 9 | Fluorescent nano-semiconductors for single particle spectroscopy. (**a**) Time series fluorescence snapshots of trapping and releasing events of 35 nm QDs on graphene oxide. (**b**) Plot of luminescence intensity of trapped QD with time. The decrease in the emission of the QD on graphene oxide with time can be clearly observed. Evolution of emission peak intensity for trapped (**c**) QD@SiO_2 with only SiO_2 shell and (**d**) pQD@SiO_2 with sulfur and SiO_2 shells. Insets: diagram of trapped (c) QD@SiO_2 and (d) pQD@SiO_2. Figure reproduced with permission from: (a, b) ref.[121], Copyright 2020 American Chemical Society; (c, d) ref.[122], Copyright 2017 American Chemical Society.

to vicinity of labeled Jurkat cell by the trapping laser. The radiative energy transfer happened between QDs (donors) and fluorescent dyed cells (acceptors). When the QD was trapped far (~10 μm) from the Jurkat cell, the emission line shape (black) equaled that of QD (red) in the spectrofluorometer (Fig. 10(b)). The same line shape was collected even when the QD540@SiO_2 approached the Jurkat cell up to a few microns (Fig. 10(c)). If the QD was trapped close to the cell within 1 μm, Alexa Fluor 546 emission from the cell dominated the recorded signal due to radiative energy transfer (Fig. 10(d, e)). Despite the low efficiency of this method, it is effective to collect fluorescence signals in far field at relatively low dye concentration. The low energy transfer efficiency also prevents the biological damage and dye photobleaching effects.

Fluorescent nanodiamonds

The fluorescence of nanodiamonds (NDs) is caused by point-defects in the diamond structure, known as color centers. The nitrogen-vacancy (NV^-), the most studied defect in NDs, consists of a nitrogen atom replacing a carbon atom, and a vacancy on a neighboring lattice site. Spin-preserving optical transitions between the ground and the excited states in the NV^- center have different relaxation pathways depending on the initial spin state, allowing them to be distinguished through optical spectroscopy. The NV^- of a ND can be excited by a light source with a specific wavelength and emit stable fluorescence. In addition, as the existence of extra magnetic field can cause NV^- ground energy level splitting, the optical properties can couple with external magnetic field. The spin-dependent fluorescent readout of ground-state electron-spin resonance (ESR) transitions in NV^- has been used for magnetic[126,127], electric[128], and thermal[129] metrology at the nanoscale. The photostability and biocompatibility of NDs[130,131] have also permitted to image and characterize NV^- centers within living cells[132], pointing to potential applications in sensing, tracking, and tagging in submicron biophysical systems.

Combination of OTs and the luminescence generated by ND has allowed quantum sensing at the single particle level. The first demonstration of optical trapping of NDs ensembles by optical trapping in liquid was published by V. R. Horowitz et al.[133]. The commercial 100-nm NDs were irradiated and annealed to contain ~500 NV^- centers in one nanocrystal. The optical trapping was performed with a 1064 nm continuous wave laser while a separate 532 nm continuous wave laser was used for optical excitation of the NV^- centers. They were able to measure spectral changes in the presence of an external magnetic field, thereby demonstrating the first magnetometry-based sensing on an ensemble of NDs, obtaining a direct current (DC) magnetic field sensitivity of 50 $\mu T/\sqrt{Hz}$ at a magnetic field of 5*G*. R. Quidant research group applied optical trapping to deterministically trap and to manipulate in three dimensions an individual ND hosting a single NV^- center[134]. The optical trapping of a single ND was proven by using a high sensitivity fluorescence camera that allows real time monitoring of the diffusion of the ND. Quidant and co-workers were able to perform vectorial magnetometry on a single

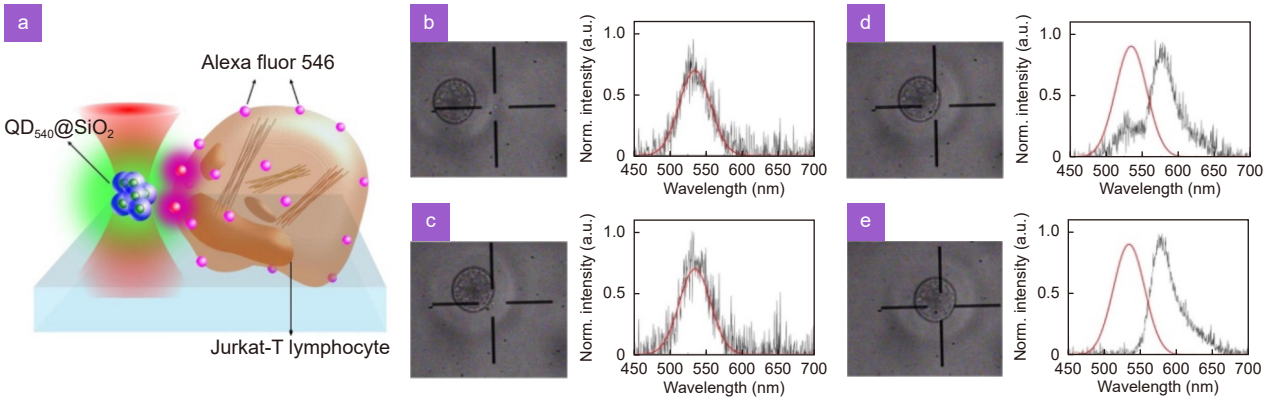

Fig. 10 | Fluorescent nano-semiconductors for cell imaging. (**a**) Sketch of the indirect excitation of a dye labeled cell. An optically trapped $QD_{540}@SiO_2$ cluster is positioned in the vicinity of a labeled Jurkat cell with Alexa Fluor 546 to induce its photoluminescence. Bright field microscopy images and collected spectra (black curves) from a $QD_{540}@SiO_2$ cluster trapped (**b**) ~10 μm away from the Jurkat cell, (**c**) close (a few microns) to the labeled Jurkat cell membrane, (**d**) in the vicinity (within 1 μm) of the Jurkat cell membrane, and (**e**) above the whole Jurkat cell structure. The optical trap position roughly matches the reticle center. Red curves represent in all cases the emission of the original $QD_{540}@SiO_2$. Figure reproduced with permission from ref.[125], Copyright 2019 American Chemical Society.

electron spin, by varying the three-dimensional magnetic field orientation, used to determine the NV^- axis, while the NV^- axis was also rotated using the electric field polarization of the trapping beam. The achieved DC magnetic field sensitivity in this configuration was improved to 40 $\mu T/\sqrt{Hz}$.

For temperature sensing application, B. Li group followed an interesting approach based on the NDs aggregation into a microsphere[135]. The authors demonstrated that the NDs can be aggregated using optical forces in liquid medium to form a microsphere, whose size, rates of formation and stabilization are related to the NDs concentration, trapping laser power, and duration of irradiation. Then, the NDs microaggregates remained stable after the laser was turned off. To perform intracellular thermometry, the NDs were incorporated into the cell by endocytosis process and then, the NDs microaggregates were formed intracellularly by using optical forces. The main advantage of the NDs aggregation and electromagnetic resonance between individual nanodiamonds is that they lead to a sevenfold intensity enhancement of 546-nm laser excitation. OT allows precise patterning and positioning the NDs microaggregates within the cell. Here, the optical trapping was performed with a 1064 nm laser and an additional 546 nm beam was used for optical excitation of the NV^- centers. Comparing to liquid solution, to form a stable NDs microaggregates in the complex intracellular environment, it required a higher trapping laser power (150 mW) and longer duration of irradiation (180 s). Under this condition, the NDs aggregates also remained stable after the laser was turned off. Then, intracellular thermal probing was demonstrated by measuring the fluorescence signal from aggregated NDs microspheres at different locations within a human brain microvascular endothelial cell (HMEC-1). First, after 24 h (Fig. 11(a)), the endothelial cells were marked to visualize the mitochondria (Fig. 11(b)). Then, the NDs were intracellularly aggregated at different locations after 180 s of irradiation (Fig. 11(c)). Temperature calibration inside cell was performed by measuring the luminescence of several NDs microspheres, between 20 °C and 60 °C. The zero-phonon line of the NDs aggregated provided a thermal shift of 25 °C nm^{-1}, with a minimum temperature difference (ΔT_{min}) of 0.5 °C at the desired locations. In addition, temperature reading was performed at different positions inside the cell: close to the nuclear membrane and the outer membrane, indicated by I and II in Fig. 11(c), respectively. This experiment revealed that the temperature at the nucleus was 2.5 °C higher than that at the membrane, what the authors explained because most of the energy-generating mitochondria stained were gathered around the nucleus[136].

Conclusions and perspectives

In summary, this review article reveals how the combination of optical trapping and colloidal optical nanoparticles has emerged great potential during the last years. Optical tweezers allow long-term immobilization and manipulation of individual optical nanoparticles in liquid media. In this respect, this makes optical tweezers a unique technology that overcomes other approaches capable of single particle studies. In those approaches, single particle isolation and manipulation requires either the use of dried samples or the physical contact between the studied particle and the detection system (such as scanning near field optical microscopy (SNOM) or atomic force microscopy (AFM)). Numerous examples described in this work (such as scanning experiments in the surroundings of microelectronic devices or living cells[106,125]) pointed out how this single particle isolation and study is possible by using rather simple and cost-effective experimental approaches. In most of the cases only a low power diode laser, a fiber coupled spectrometer, and a conventional microscope objective are required to make single particle studies possible even in laboratories with reduced access to tip-scanning technologies. In this sense, we are firmly convinced that in the near future optical tweezers will become an increasingly popular tool for single particle studies.

Despite the great potential of optical tweezers for single particle studies, this field is still in its infancy. For most of the research groups working on optical particles, this technique is still considered as a limited technology. In our opinion, it is because there are some fundamental questions that are still open and not faced as most of the works focus on applications rather than filling the gaps of knowledge. For instance, there is a lack of a precise formula that describes the optical forces acting on colloidal particles in a realistic way. Optical forces are typically calculated and described considering a homogeneous particle surrounded by a liquid medium. This is an oversimplification of the real situation, as the surface of colloidal nanoparticles is complex since decoration with organic ligands is required for them to be stable. Controlled trapping and manipulation require a full

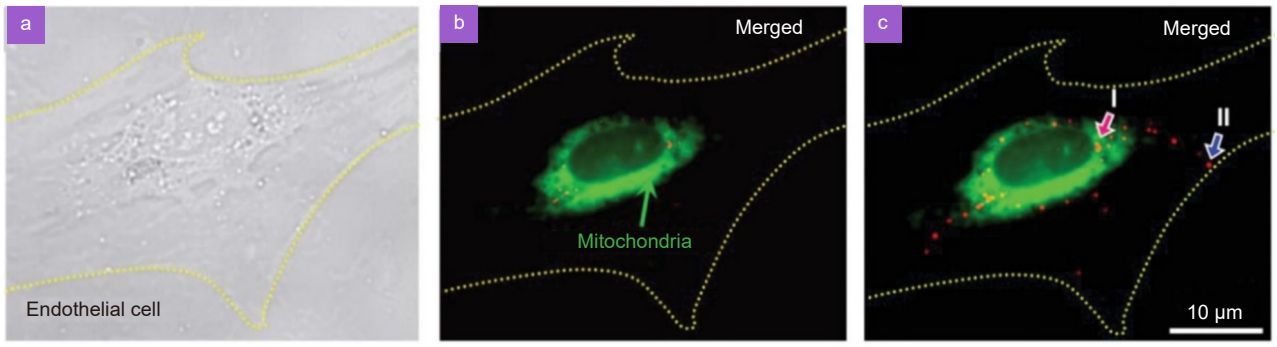

Fig. 11 | Fluorescent nanodiamonds for cell imaging. (**a**) Confocal microscope image of a human brain microvascular endothelial cell (HMEC-1). (**b**) Fluorescence image of the cell with mitochondria stained by Mito-Tracker Green FM (excitation: 490 nm, emission: 516 nm). (**c**) Fluorescence image of the nanodiamonds microaggregates at different locations in the HMEC-1. Blue and pink arrows pointed to the microspheres near the nuclear membrane and cell membrane, respectively. Figure reproduced from ref.[135], under a Creative Commons Attribution License.

understanding on the role played by surface functionalization in the optical forces.

Another fundamental question that remains open is the actual spatial resolution that can be achieved when an optically trapped particle is used for remote sensing. This question is not typically addressed as it is considered that the particle is stably trapped at the laser focus, so the spatial resolution is assumed to be given by the size of the sensing particle during remote sensing experiments. But this is not the case, especially for nanoparticles. In these conditions, experimental works have demonstrated how thermal energy is comparable to the depth of the optical potential well[30,45]. Thus, Brownian motion and the position of the sensing nanoparticle oscillates in the surroundings of the laser focus are not negligible. Consequently, the sensing readout corresponds to an average over the volume covered by the motion of the nanoparticle. If this technology is to be driven to its limits, achieving actual submicrometric resolution, the Brownian motion within the trap must be minimized. This can be achieved by increasing the optical forces acting on the nanoparticles. As mentioned in Section *Introduction*, there are two ways to improve the optical forces. On one side, the optical forces can be improved by designing new optical systems to enhance the electric field[36,41,137,138]. On the other side, optical forces can be tailored by an adequate design of the optical nanoparticles[11,33,34]. Here we identify different directions. Core-shell engineering[139,140] allows the fabrication of hybrid systems that, for instance, could allow the combination of plasmonic shells (with high polarizability and, hence, creating large optical forces) with luminescent cores (in charge of sensing). At the same time, as already mentioned, adequate surface tailoring could be also explored to improve optical forces by increasing the electronic polarizability of the nanoparticle-medium interface[33,34]. In addition, adjusting nanoparticle doping has also been revealed as an efficient way for improving nanoparticle polarizability and optical forces[68]. This possibility has been explored only in lanthanide-doped nanoparticles, but we believe that would be also valid for other optical nanoparticles studied in this review such as quantum dots and semiconductor nanoparticles.

This review article evidences that remote sensing is one of the most promising applications of optically trapped single particles. It is demonstrated how optical tweezers allow remote thermal and chemical three-dimensional sensing. Results highlighted in this review are promising, but must be considered as preliminary, as they do not consider the possible presence of bias. That is an issue that should be considered in any sensing experiment. It has been revealed of special importance in thermal sensing experiments[24,141]. Chemical changes in the particle environment can cause changes in their optical properties that can be erroneous attributed to temperature fluctuations. In addition, the laser-induced self-heating of the nanoparticle could also give erroneous thermal readouts[44]. If we want optically trapped nanoparticles to be considered by the scientific community as reliable sensors, it is imperative to start studying the presence of bias mechanisms at the single particle level by establishing standardized procedures.

Finally, most of the works included in this review are based on a quite simple analysis of the optical signal provided by individual particles within an optical trap. So far, this has been a valid approach that has allowed particle tracking and remote sensing. In some cases, the analysis is as simple as recording the fluorescence

intensity generated within the trap. Nowadays, advanced analysis methods based on Artificial Intelligence are being used for more accurate and reliable sensing[142,143]. In this case, the analysis of the optical signal becomes more complicated, but it is worthy as it would allow accurate, reliable, and multiparametric sensing without requiring a sophistication in the experimental setup or without the need of developing new materials.

References

1. Li Y, Lin CJ, Li KQ, Chi C, Huang BL. Nanoparticle-on-mirror metamaterials for full-spectrum selective solar energy harvesting. *Nano Lett* **22**, 5659–5666 (2022).
2. Kameya Y, Hanamura K. Enhancement of solar radiation absorption using nanoparticle suspension. *Solar Energy* **85**, 299–307 (2011).
3. Zhang M, Lin YJ, Mullen TJ, Lin WF, Sun LD et al. Improving hematite's solar water splitting efficiency by incorporating rare-earth upconversion nanomaterials. *J Phys Chem Lett* **3**, 3188–3192 (2012).
4. Ma DY, Shen YL, Su TT, Zhao J, Rahman NU et al. Performance enhancement in up-conversion nanoparticle-embedded perovskite solar cells by harvesting near-infrared sunlight. *Mater Chem Front* **3**, 2058–2065 (2019).
5. Zuo MZ, Qian WR, Li TH, Hu XY, Jiang JL et al. Full-color tunable fluorescent and chemiluminescent supramolecular nanoparticles for anti-counterfeiting inks. *ACS Appl Mater Interfaces* **10**, 39214–39221 (2018).
6. Przybylska D, Grzyb T, Erdman A, Olejnik K, Szczeszak A. Anti-counterfeiting system based on luminescent varnish enriched by NIR- excited nanoparticles for paper security. *Sci Rep* **12**, 19388 (2022).
7. Kumar P, Dwivedi J, Gupta BK. Highly luminescent dual mode rare-earth nanorod assisted multi-stage excitable security ink for anti-counterfeiting applications. *J Mater Chem C* **2**, 10468–10475 (2014).
8. Deng Y, Ediriwickrema A, Yang F, Lewis J, Girardi M et al. A sunblock based on bioadhesive nanoparticles. *Nat Mater* **14**, 1278–1285 (2015).
9. Huang J, He YR, Wang L, Huang YM, Jiang BC. Bifunctional Au@TiO_2 core-shell nanoparticle films for clean water generation by photocatalysis and solar evaporation. *Energy Convers Manag* **132**, 452–459 (2017).
10. Jaque D, Martínez Maestro L, del Rosal B, Haro-Gonzalez P, Benayas A et al. Nanoparticles for photothermal therapies. *Nanoscale* **6**, 9494–9530 (2014).
11. Lu DS, Retama JR, Marin R, Marqués MI, Calderón OG et al. Thermoresponsive polymeric nanolenses magnify the thermal sensitivity of single upconverting nanoparticles. *Small* **18**, 2202452 (2022).
12. López-Peña G, Hamraoui K, Horchani-Naifer K, Gerke C, Ortgies DH et al. Lanthanide doped nanoheaters with reliable and absolute temperature feedback. *Phys B Condens Matter* **631**, 413652 (2022).
13. Shen YL, Lifante J, Zabala-Gutierrez I, de la Fuente-Fernández M, Granado M et al. Reliable and remote monitoring of absolute temperature during liver inflammation via luminescence-lifetime-based nanothermometry. *Adv Mater* **34**, 2107764 (2022).
14. Rodríguez-Sevilla P, Zhang YH, Haro-González P, Sanz-Rodríguez F, Jaque F et al. Thermal scanning at the cellular level by an optically trapped upconverting fluorescent particle. *Adv Mater* **28**, 2421–2426 (2016).
15. Rodríguez-Sevilla P, Zhang YH, de Sousa N, Marqués MI, Sanz-Rodríguez F et al. Optical torques on upconverting particles for intracellular microrheometry. *Nano Lett* **16**, 8005–8014 (2016).
16. Esipova TV, Ye XC, Collins JE, Sakadžić S, Mandeville ET et al. Dendritic upconverting nanoparticles enable in vivo multiphoton microscopy with low-power continuous wave sources. *Proc Natl Acad Sci USA* **109**, 20826–20831 (2012).
17. Suresh K, Bankapur A, Chidangil S, Madhyastha H, Sa-kai K et al. A broadband optical pH sensor using upconversion luminescence. *J Mater Chem C* **9**, 8606–8614 (2021).
18. Benjaminsen RV, Sun HH, Henriksen JR, Christensen NM, Almdal K et al. Evaluating nanoparticle sensor design for intracellular pH measurements. *ACS Nano* **5**, 5864–5873 (2011).
19. Ali R, Saleh SM, Meier RJ, Azab HA, Abdelgawad II et al. Upconverting nanoparticle based optical sensor for carbon dioxide. *Sens Actuators B Chem* **150**, 126–131 (2010).
20. Kameda M, Seki H, Makoshi T, Amao Y, Nakakita K. A fast-response pressure sensor based on a dye-adsorbed silica nanoparticle film. *Sens Actuators B Chem* **171–172**, 343–349 (2012).
21. Schmidt MA, Lei DY, Wondraczek L, Nazabal V, Maier SA. Hybrid nanoparticle–microcavity-based plasmonic nanosensors with improved detection resolution and extended remote-sensing ability. *Nat Commun* **3**, 1108 (2012).
22. Huang G, Liu YT, Wang DJ, Zhu Y, Wen SH et al. Upconversion nanoparticles for super-resolution quantification of single small extracellular vesicles. *eLight* **2**, 20 (2022).
23. Rodríguez-Sevilla P, Rodríguez-Rodríguez H, Pedroni M, Speghini A, Bettinelli M et al. Assessing single upconverting nanoparticle luminescence by optical tweezers. *Nano Lett* **15**, 5068–5074 (2015).
24. Labrador-Páez L, Pedroni M, Speghini A, García-Solé J, Haro-González P et al. Reliability of rare-earth-doped infrared luminescent nanothermometers. *Nanoscale* **10**, 22319–22328 (2018).
25. Katano S, Hotsuki M, Uehara Y. Creation and luminescence of a single silver nanoparticle on Si(111) investigated by scanning tunneling microscopy. *J Phys Chem C* **120**, 28575–28582 (2016).
26. Silly F, Gusev AO, Charra F, Taleb A, Pileni MP. Scanning tunneling microscopy-controlled dynamic switching of single nanoparticle luminescence at room temperature. *Appl Phys Lett* **79**, 4013–4015 (2001).
27. Schietinger S, Aichele T, Wang HQ, Nann T, Benson O. Plasmon-enhanced upconversion in single $NaYF_4$: Yb^{3+}/Er^{3+} codoped nanocrystals. *Nano Lett* **10**, 134–138 (2010).
28. Tong LM, Li ZP, Zhu T, Xu HX, Liu ZF. Single gold-nanoparticle-enhanced raman scattering of individual single-walled carbon nanotubes via atomic force microscope manipulation. *J Phys Chem C* **112**, 7119–7123 (2008).
29. Ratchford D, Shafiei F, Kim S, Gray SK, Li XQ. Manipulating coupling between a single semiconductor quantum dot and single gold nanoparticle. *Nano Lett* **11**, 1049–1054 (2011).

30. Lu DS, Labrador-Páez L, Ortiz-Rivero E, Frades P, Antoniak MA et al. Exploring single-nanoparticle dynamics at high temperature by optical tweezers. *Nano Lett* **20**, 8024–8031 (2020).
31. Ashkin A. Acceleration and trapping of particles by radiation pressure. *Phys Rev Lett* **24**, 156–159 (1970).
32. Dienerowitz M, Mazilu M, Dholakia K. Optical manipulation of nanoparticles: a review. *J Nanophotonics* **2**, 021875 (2008).
33. Rodríguez-Sevilla P, Prorok K, Bednarkiewicz A, Marqués MI, García-Martín A et al. Optical forces at the nanoscale: size and electrostatic effects. *Nano Lett* **18**, 602–609 (2018).
34. Rodríguez-Rodríguez H, Sevilla PR, Rodríguez EM, Ortgies DH, Pedroni M et al. Enhancing optical forces on fluorescent up-converting nanoparticles by surface charge tailoring. *Small* **11**, 1555–1561 (2015).
35. Berthelot J, Aćimović SS, Juan ML, Kreuzer MP, Renger J et al. Three-dimensional manipulation with scanning near-field optical nanotweezers. *Nat Nanotechnol* **9**, 295–299 (2014).
36. Grigorenko AN, Roberts NW, Dickinson MR, Zhang Y. Nanometric optical tweezers based on nanostructured substrates. *Nat Photonics* **2**, 365–370 (2008).
37. Han X, Truong VG, Thomas PS, Chormaic SN. Sequential trapping of single nanoparticles using a gold plasmonic nanohole array. *Photonics Res* **6**, 981–986 (2018).
38. Mandal S, Serey X, Erickson D. Nanomanipulation using silicon photonic crystal resonators. *Nano Lett* **10**, 99–104 (2010).
39. Wang HT, Wu X, Shen DY. Localized optical manipulation in optical ring resonators. *Opt Express* **23**, 27650–27660 (2015).
40. Lu DS, Pedroni M, Labrador-Páez L, Marqués MI, Jaque D et al. Nanojet trapping of a single sub-10 nm upconverting nanoparticle in the full liquid water temperature range. *Small* **17**, 2006764 (2021).
41. Li YC, Xin HB, Lei HX, Liu LL, Li YZ et al. Manipulation and detection of single nanoparticles and biomolecules by a photonic nanojet. *Light Sci Appl* **5**, e16176 (2016).
42. Chen ZZ, Cai ZW, Liu WB, Yan ZJ. Optical trapping and manipulation for single-particle spectroscopy and microscopy. *J Chem Phys* **157**, 050901 (2022).
43. Svoboda K, Block SM. Optical trapping of metallic Rayleigh particles. *Opt Lett* **19**, 930–932 (1994).
44. Lehmuskero A, Johansson P, Rubinsztein-Dunlop H, Tong LM, Käll M. Laser trapping of colloidal metal nanoparticles. *ACS Nano* **9**, 3453–3469 (2015).
45. Lu DS, Gámez F, Haro-González P. Temperature effects on optical trapping stability. *Micromachines* **12**, 954 (2021).
46. Shao L, Käll M. Light‐driven rotation of plasmonic nanomotors. *Adv Funct Mater* **28**, 1706272 (2018).
47. Yuan YF, Lin YN, Gu BB, Panwar N, Tjin SC et al. Optical trapping-assisted SERS platform for chemical and biosensing applications: design perspectives. *Coord Chem Rev* **339**, 138–152 (2017).
48. Ohlinger A, Nedev S, Lutich AA, Feldmann J. Optothermal escape of plasmonically coupled silver nanoparticles from a three-dimensional optical trap. *Nano Lett* **11**, 1770–1774 (2011).
49. Andrén D, Shao L, Laïnk NO, Aćimović SS, Johansson P et al. Probing photothermal effects on optically trapped gold nanorods by simultaneous plasmon spectroscopy and brownian dynamics analysis. *ACS Nano* **11**, 10053–10061 (2017).
50. Andres-Arroyo A, Wang F, Toe WJ, Reece P. Intrinsic heating in optically trapped Au nanoparticles measured by dark-field spectroscopy. *Biomed Opt Express* **6**, 3646–3654 (2015).
51. Rodrigo JA, Alieva T. Polymorphic beams and Nature inspired circuits for optical current. *Sci Rep* **6**, 35341 (2016).
52. Guffey MJ, Scherer NF. All-optical patterning of Au nanoparticles on surfaces using optical traps. *Nano Lett* **10**, 4302–4308 (2010).
53. Ling L, Huang L, Fu JX, Guo HL, Li JF et al. The properties of gold nanospheres studied with dark field optical trapping. *Opt Express* **21**, 6618–6624 (2013).
54. Yang F, Yang NN, Huo XY, Xu SY. Thermal sensing in fluid at the micro-nano-scales. *Biomicrofluidics* **12**, 041501 (2018).
55. del Rosal B, Ximendes E, Rocha U, Jaque D. In vivo luminescence nanothermometry: from materials to applications. *Adv Opt Mater* **5**, 1600508 (2017).
56. Zhou HY, Sharma M, Berezin O, Zuckerman D, Berezin MY. Nanothermometry: from microscopy to thermal treatments. *ChemPhysChem* **17**, 27–36 (2016).
57. Setoura K, Okada Y, Werner D, Hashimoto S. Observation of nanoscale cooling effects by substrates and the surrounding media for single gold nanoparticles under CW-laser illumination. *ACS Nano* **7**, 7874–7885 (2013).
58. Hajizadeh F, Shao L, Andrén D, Johansson P, Rubinsztein-Dunlop H et al. Brownian fluctuations of an optically rotated nanorod. *Optica* **4**, 746–751 (2017).
59. Zohar N, Chuntonov L, Haran G. The simplest plasmonic molecules: metal nanoparticle dimers and trimers. *J Photochem Photobiol C Photochem Rev* **21**, 26–39 (2014).
60. Kermani H, Rohrbach A. Orientation-control of two plasmonically coupled nanoparticles in an optical trap. *ACS Photonics* **5**, 4660–4667 (2018).
61. Blattmann M, Rohrbach A. Plasmonic coupling dynamics of silver nanoparticles in an optical trap. *Nano Lett* **15**, 7816–7821 (2015).
62. Rodrigo JA, Angulo M, Alieva T. All-optical motion control of metal nanoparticles powered by propulsion forces tailored in 3D trajectories. *Photonics Res* **9**, 1–12 (2021).
63. Sönnichsen C, Reinhard BM, Liphardt J, Alivisatos AP. A molecular ruler based on plasmon coupling of single gold and silver nanoparticles. *Nat Biotechnol* **23**, 741–745 (2005).
64. Han F, Armstrong T, Andres-Arroyo A, Bennett D, Soeriyadi A et al. Optical tweezers-based characterisation of gold core–satellite plasmonic nano-assemblies incorporating thermo-responsive polymers. *Nanoscale* **12**, 1680–1687 (2020).
65. König K. Multiphoton microscopy in life sciences. *J Microsc* **200**, 83–104 (2000).
66. Vetrone F, Naccache R, Zamarrón A, de la Fuente AJ, Sanz-Rodríguez F et al. Temperature sensing using fluorescent nanothermometers. *ACS Nano* **4**, 3254–3258 (2010).
67. Haro-González P, del Rosal B, Maestro LM, Rodríguez EM, Naccache R et al. Optical trapping of $NaYF_4$: Er^{3+}, Yb^{3+} upconverting fluorescent nanoparticles. *Nanoscale* **5**, 12192–12199 (2013).
68. Shan XC, Wang F, Wang DJ, Wen SH, Chen CH et al. Optical tweezers beyond refractive index mismatch using highly doped upconversion nanoparticles. *Nat Nanotechnol* **16**, 531–537 (2021).
69. Cantelar E, Cussó F. Dynamics of the Yb^{3+} to Er^{3+} energy transfer in $LiNbO_3$. *Appl Phys B* **69**, 29–33 (1999).
70. Cao BS, He YY, Feng ZQ, Li YS, Dong B. Optical temperature

sensing behavior of enhanced green upconversion emissions from Er–Mo: $Yb_2Ti_2O_7$ nanophosphor. *Sens Actuators B Chem* **159**, 8–11 (2011).
71. Petit J, Viana B, Goldner P. Internal temperature measurement of an ytterbium doped material under laser operation. *Opt Express* **19**, 1138–1146 (2011).
72. Quintanilla M, Cantelar E, Cussó F, Villegas M, Caballero AC. Temperature sensing with up-converting submicron-sized $LiNbO_3$: Er^{3+}/Yb^{3+} particles. *Appl Phys Express* **4**, 022601 (2011).
73. Alencar MARC, Maciel GS, Araújo CBd, Patra A. Er^{3+}-doped $BaTiO_3$ nanocrystals for thermometry: influence of nanoenvironment on the sensitivity of a fluorescence based temperature sensor. *Appl Phys Lett* **84**, 4753–4755 (2004).
74. Haro-González P, Martín IR, Martín LL, León-Luis SF, Pérez-Rodríguez C et al. Characterization of Er^{3+} and Nd^{3+} doped Strontium Barium Niobate glass ceramic as temperature sensors. *Opt Mater* **33**, 742–745 (2011).
75. Cai ZP, Xu HY. Point temperature sensor based on green upconversion emission in an Er: ZBLALiP microsphere. *Sens Actuators A Phys* **108**, 187–192 (2003).
76. Vetrone F, Naccache R, de la Fuente AJ, Sanz-Rodríguez F, Blazquez-Castro A et al. Intracellular imaging of HeLa cells by non-functionalized $NaYF_4$: Er^{3+}, Yb^{3+} upconverting nanoparticles. *Nanoscale* **2**, 495–498 (2010).
77. Maestro LM, Rodríguez EM, Vetrone F, Naccache R, Loro H et al. Nanoparticles for highly efficient multiphoton fluorescence bioimaging. *Opt Express* **18**, 23544–23553 (2010).
78. Chatterjee DK, Rufaihah AJ, Zhang Y. Upconversion fluorescence imaging of cells and small animals using lanthanide doped nanocrystals. *Biomaterials* **29**, 937–943 (2008).
79. Wang M, Mi CC, Wang WX, Liu CH, Wu YF et al. Immunolabeling and NIR-excited fluorescent imaging of HeLa cells by using $NaYF_4$: Yb, Er upconversion nanoparticles. *ACS Nano* **3**, 1580–1586 (2009).
80. Drobczyński S, Prorok K, Tamarov K, Duś-Szachniewicz K, Lehto VP et al. Toward controlled photothermal treatment of single cell: optically induced heating and remote temperature monitoring in vitro through double wavelength optical tweezers. *ACS Photonics* **4**, 1993–2002 (2017).
81. Liu TY, Liu XG, Spring DR, Qian XH, Cui JN et al. Quantitatively mapping cellular viscosity with detailed organelle information via a designed PET fluorescent probe. *Sci Rep* **4**, 5418 (2014).
82. Wirtz D. Particle-tracking microrheology of living cells: principles and applications. *Ann Rev Biophys* **38**, 301–326 (2009).
83. Lammerding J, Lee RT. The nuclear membrane and mechanotransduction: impaired nuclear mechanics and mechanotransduction in lamin A/C deficient cells. *Novartis Found Symp* **264**, 264–273 (2005).
84. Lammerding J, Schulze PC, Takahashi T, Kozlov S, Sullivan T et al. Lamin A/C deficiency causes defective nuclear mechanics and mechanotransduction. *J Clin Invest* **113**, 370–378 (2004).
85. Lee JSH, Chang MI, Tseng Y, Wirtz D. Cdc42 mediates nucleus movement and MTOC polarization in Swiss 3T3 fibroblasts under mechanical shear stress. *Mol Biol Cell* **16**, 871–880 (2005).
86. Minin AA, Kulik AV, Gyoeva FK, Li Y, Goshima G et al. Regulation of mitochondria distribution by RhoA and formins. *J Cell Sci* **119**, 659–670 (2006).
87. Kuimova MK. Mapping viscosity in cells using molecular rotors. *Phys Chem Chem Phys* **14**, 12671–12686 (2012).
88. Nadiv O, Shinitzky M, Manu H, Hecht D, Roberts CT Jr et al. Elevated protein tyrosine phosphatase activity and increased membrane viscosity are associated with impaired activation of the insulin receptor kinase in old rats. *Biochem J* **298**, 443–450 (1994).
89. Deliconstantinos G, Villiotou V, Stavrides JC. Modulation of particulate nitric oxide synthase activity and peroxynitrite synthesis in cholesterol enriched endothelial cell membranes. *Biochem Pharmacol* **49**, 1589–1600 (1995).
90. Zubenko GS, Kopp U, Seto T, Firestone LL. Platelet membrane fluidity individuals at risk for Alzheimer's disease: a comparison of results from fluorescence spectroscopy and electron spin resonance spectroscopy. *Psychopharmacology* **145**, 175–180 (1999).
91. Chen P, Song M, Wu E, Wu BT, Zhou JJ et al. Polarization modulated upconversion luminescence: single particle *vs*. few-particle aggregates. *Nanoscale* **7**, 6462–6466 (2015).
92. Rodríguez-Sevilla P, Labrador-Páez L, Wawrzyńczyk D, Nyk M, Samoć M et al. Determining the 3D orientation of optically trapped upconverting nanorods by *in situ* single-particle polarized spectroscopy. *Nanoscale* **8**, 300–308 (2016).
93. Lyu Z-, Dong H, Yang XF, Sun LD, Yan CH. Highly polarized upconversion emissions from lanthanide-doped $LiYF_4$ crystals as spatial orientation indicators. *J Phys Chem Lett* **12**, 11288–11294 (2021).
94. Green KK, Wirth J, Lim SF. Nanoplasmonic upconverting nanoparticles as orientation sensors for single particle microscopy. *Sci Rep* **7**, 762 (2017).
95. Kim J, Chacón R, Wang ZJ, Larquet E, Lahlil K et al. Measuring 3D orientation of nanocrystals via polarized luminescence of rare-earth dopants. *Nat Commun* **12**, 1943 (2021).
96. Chakraborty S, Nandi S, Bhattacharyya K, Mukherjee S. Probing viscosity of co-polymer hydrogel and hela cell using fluorescent gold nanoclusters: fluorescence correlation spectroscopy and anisotropy decay. *ChemPhysChem* **21**, 406–414 (2020).
97. Ramazanova I, Suslov M, Sibgatullina G, Petrov K, Fedorenko S et al. Determination of the viscosity of the cytoplasm of M-HeLa cells using fluorescent magnetic nanoparticles and an electromagnetic needle, 30 August 2022, PREPRINT (Version 1) available at Research Square. https://doi.org/10.21203/rs.3.rs-1994074/v1
98. Schäferling M. Nanoparticle-based luminescent probes for intracellular sensing and imaging of pH. *Wiley Interdiscip Rev Nanomed Nanobiotechnol* **8**, 378–413 (2016).
99. Liu J, Zheng M, Xiong ZJ, Li ZY. 3D dynamic motion of a dielectric micro-sphere within optical tweezers. *Opto-Electron Adv* **4**, 200015 (2021).
100. Kim K, Yoon J, Park YK. Simultaneous 3D visualization and position tracking of optically trapped particles using optical diffraction tomography. *Optica* **2**, 343–346 (2015).
101. Bresolí-Obach R, Kudo T, Louis B, Chang YC, Scheblykin IG et al. Resonantly enhanced optical trapping of single dye-doped particles at an interface. *ACS Photonics* **8**, 1832–1839 (2021).
102. Louis B, Huang CH, Camacho R, Scheblykin IG, Sugiyama T et al. Unravelling 3D dynamics and hydrodynamics during in-

corporation of dielectric particles to an optical trapping site. *ACS Nano* **17**, 3797–3808 (2023).
103. Ito S, Mitsuishi M, Setoura K, Tamura M, Iida T et al. Mesoscopic motion of optically trapped particle synchronized with photochromic reactions of diarylethene derivatives. *J Phys Chem Lett* **9**, 2659–2664 (2018).
104. Hosokawa C, Tsuji T, Kishimoto T, Okubo T, Kudoh SN et al. Convection dynamics forced by optical trapping with a focused laser beam. *J Phys Chem C* **124**, 8323–8333 (2020).
105. Florin EL, Horber JKH, Stelzer EHK. High-resolution axial and lateral position sensing using two-photon excitation of fluorophores by a continuous-wave Nd: YAG laser. *Appl Phys Lett* **69**, 446–448 (1996).
106. Florin EL, Pralle A, Horber JKH, Stelzer EHK. Photonic force microscope based on optical tweezers and two-photon excitation for biological applications. *J Struct Biol* **119**, 202–211 (1997).
107. Lang MJ, Fordyce PM, Block SM. Combined optical trapping and single-molecule fluorescence. *J Biol* **2**, 6 (2003).
108. Lang MJ, Fordyce PM, Engh AM, Neuman KC, Block SM. Simultaneous, coincident optical trapping and single-molecule fluorescence. *Nat Methods* **1**, 133–139 (2004).
109. Zhang CY, Yeh HC, Kuroki MT, Wang TH. Single-quantum-dot-based DNA nanosensor. *Nat Mater* **4**, 826–831 (2005).
110. Wang LJ, Luo ML, Zhang QY, Tang B, Zhang CY. Single quantum dot-based nanosensor for rapid and sensitive detection of terminal deoxynucleotidyl transferase. *Chem Commun* **53**, 11016–11019 (2017).
111. Zhang Y, Zhang CY. Sensitive detection of microRNA with isothermal amplification and a single-quantum-dot-based nanosensor. *Anal Chem* **84**, 224–231 (2012).
112. Michalet X, Pinaud FF, Bentolila LA, Tsay JM, Doose S et al. Quantum dots for live cells, in vivo imaging, and diagnostics. *Science* **307**, 538–544 (2005).
113. Pan LY, Ishikawa A, Tamai N. Detection of optical trapping of CdTe quantum dots by two-photon-induced luminescence. *Phys Rev B* **75**, 161305 (2007).
114. Jauffred L, Richardson AC, Oddershede LB. Three-dimensional optical control of individual quantum dots. *Nano Lett* **8**, 3376–3380 (2008).
115. Jauffred L, Oddershede LB. Two-photon quantum dot excitation during optical trapping. *Nano Lett* **10**, 1927–1930 (2010).
116. Jauffred L, Kyrsting A, Arnspang EC, Reihani SNS, Oddershede LB. Sub-diffraction positioning of a two-photon excited and optically trapped quantum dot. *Nanoscale* **6**, 6997–7003 (2014).
117. Xu Z, Crozier KB. All-dielectric nanotweezers for trapping and observation of a single quantum dot. *Opt Express* **27**, 4034–4045 (2019).
118. Chiang WY, Okuhata T, Usman A, Tamai N, Masuhara H. Efficient optical trapping of CdTe quantum dots by femtosecond laser pulses. *J Phys Chem B* **118**, 14010–14016 (2014).
119. Head CR, Kammann E, Zanella M, Manna L, Lagoudakis PG. Spinningnanorods - active optical manipulation of semiconductor nanorods using polarised light. *Nanoscale* **4**, 3693–3697 (2012).
120. Agarwal R, Ladavac K, Roichman Y, Yu GH, Lieber CM et al. Manipulation and assembly of nanowires with holographic optical traps. *Opt Express* **13**, 8906–8912 (2005).
121. Pinapati P, Joby JP, Cherukulappurath S. Graphene oxide based two-dimensional optical tweezers for low power trapping of quantum dots and *E. coli* bacteria. *ACS Appl Nano Mater* **3**, 5107–5115 (2020).
122. Rodríguez-Rodríguez H, Acebrón M, Juárez BH, Arias-Gonzalez JR. Luminescence dynamics of silica-encapsulated quantum dots during optical trapping. *J Phys Chem C* **121**, 10124–10130 (2017).
123. Pauzauskie PJ, Radenovic A, Trepagnier E, Shroff H, Yang PD et al. Optical trapping and integration of semiconductor nanowire assemblies in water. *Nat Mater* **5**, 97–101 (2006).
124. Nakayama Y, Pauzauskie PJ, Radenovic A, Onorato RM, Saykally RJ et al. Tunable nanowire nonlinear optical probe. *Nature* **447**, 1098–1101 (2007).
125. Rodríguez-Rodríguez H, Acebrón M, Iborra FJ, Arias-Gonzalez JR, Juárez BH. Photoluminescence activation of organic dyes *via* optically trapped quantum dots. *ACS Nano* **13**, 7223–7230 (2019).
126. Taylor JM, Cappellaro P, Childress L, Jiang L, Budker D et al. High-sensitivity diamond magnetometer with nanoscale resolution. *Nat Phys* **4**, 810–816 (2008).
127. Balasubramanian G, Chan IY, Kolesov R, Al-Hmoud M, Tisler J et al. Nanoscale imaging magnetometry with diamond spins under ambient conditions. *Nature* **455**, 648–651 (2008).
128. Dolde F, Fedder H, Doherty MW, Nöbauer T, Rempp F et al. Electric-field sensing using single diamond spins. *Nat Phys* **7**, 459–463 (2011).
129. Toyli DM, Christle DJ, Alkauskas A, Buckley BB, Van de Walle CG et al. Measurement and control of single nitrogen-vacancy center spins above 600 K. *Phys Rev X* **2**, 031001 (2012).
130. Yu SJ, Kang MW, Chang HC, Chen KM, Yu YC. Bright fluorescent nanodiamonds: No photobleaching and low cytotoxicity. *J Am Chem Soc* **127**, 17604–17605 (2005).
131. Liu KK, Cheng CL, Chang CC, Chao JI. Biocompatible and detectable carboxylated nanodiamond on human cell. *Nanotechnology* **18**, 325102 (2007).
132. McGuinness LP, Yan Y, Stacey A, Simpson DA, Hall LT et al. Quantum measurement and orientation tracking of fluorescent nanodiamonds inside living cells. *Nat Nanotechnol* **6**, 358–363 (2011).
133. Horowitz VR, Alemán BJ, Christle DJ, Cleland AN, Awschalom DD. Electron spin resonance of nitrogen-vacancy centers in optically trapped nanodiamonds. *Proc Natl Acad Sci USA* **109**, 13493–13497 (2012).
134. Geiselmann M, Juan ML, Renger J, Say JM, Brown LJ et al. Three-dimensional optical manipulation of a single electron spin. *Nat Nanotechnol* **8**, 175–179 (2013).
135. Wu TL, Chen XX, Gong ZY, Yan JH, Guo JH et al. Intracellular thermal probing using aggregated fluorescent nanodiamonds. *Adv Sci* **9**, 2103354 (2022).
136. Chrétien D, Bénit P, Ha HH, Keipert S, El-Khoury R et al. Mitochondria are physiologically maintained at close to 50 °C. *PLoS Biol* **16**, e2003992 (2018).
137. Roxworthy BJ, Toussaint KC. Optical trapping with π-phase cylindrical vector beams. *New J Phys* **12**, 073012 (2010).
138. Huang L, Guo HL, Li JF, Ling L, Feng BH et al. Optical trapping of gold nanoparticles by cylindrical vector beam. *Opt Lett* **37**, 1694–1696 (2012).
139. Zhang H, Li YJ, Ivanov IA, Qu YQ, Huang Y et al. Plasmonic modulation of the upconversion fluorescence in $NaYF_4$: Yb/Tm hexaplate nanocrystals using gold nanoparticles or nanoshells.

Angew Chem Int Ed **49**, 2865–2868 (2010).

140. Fujii M, Nakano T, Imakita K, Hayashi S. Upconversion luminescence of er and Yb codoped $NaYF_4$ nanoparticles with metal shells. *J Phys Chem C* **117**, 1113–1120 (2013).
141. Shen YL, Lifante J, Fernández N, Jaque D, Ximendes E. *In vivo* spectral distortions of infrared luminescent nanothermometers compromise their reliability. *ACS Nano* **14**, 4122–4133 (2020).
142. von Chamier L, Laine RF, Jukkala J, Spahn C, Krentzel D et al. Democratising deep learning for microscopy with ZeroCostDL4Mic. *Nat Commun* **12**, 2276 (2021).
143. Zhu MS, Zhuang J, Li Z, Liu QQ, Zhao RP et al. Machine-learning-assisted single-vessel analysis of nanoparticle permeability in tumour vasculatures. *Nat Nanotechnol* **18**, 657–666 (2023).

Acknowledgements

This work was supported by projects PID2019-106211RB-I00, PID2019-105195RA-I00, and PID2021-123228NB-I00, funded by MCIN/AEI/ 10.13039/501100011033 and projects CNS2022-135495, and TED2021-129937B-I00 funded by MCIN/AEI/ 10.13039/501100011033 and by the "European Union NextGenerationEU/PRTR. P. Camarero thanks Comunidad de Madrid for Programa Investigo by Plan de Recuperación, Transformación y Resiliencia – Comunidad de Madrid – Ministerio de Trabajo y Economía Social de España - Unión Europea - NextGenerationEU. F. Zhang acknowledges the scholarship from the China Scholarship Council (202108440235). Work was also supported by Comunidad de Madrid (S2022/BMD-7403 RENIM-CM and REACT-UCM projects).

Competing interests

The authors declare no competing financial interests.